A Change in Ligand Hapticity Promotes Lewis Base Dissociation

Supporting Information

Payton A. Fortuna‡, Leslie S. G. Kelley‡, Yipeng Sun, Jiabin Xu, Zhiqiang Wang, Paul D. Boyle, Tsun-Kong Sham, Viktor N. Staroverov*, Johanna M. Blacquiere**

Department of Chemistry
The University of Western Ontario
London, Ontario, Canada, N6A 5B7

Table of Contents

I – Experimental Procedures

General Procedures. All reactions were conducted in a nitrogen atmosphere glovebox or using standard Schlenk line techniques under an argon atmosphere, unless explicitly stated otherwise. All glassware was oven dried at 150 ˚C for at least 3 h and cooled under a nitrogen or argon atmosphere prior to use, unless otherwise stated. All reagents used were obtained from commercially available sources and used without further purification, unless otherwise indicated. Potassium hydride was purchased from Alfa Aesar as a 30%$_{w/w}$ suspension in mineral oil and was purified by filtration through a fritted funnel (conducted in a nitrogen atmosphere glovebox). The solid KH was then washed with dry hexanes and diethyl ether (20 mL/g KH) and dried under vacuum. The following materials were prepared following literature procedures: [PdCl(CH_3)(COD)][1] and 2′-(diphenylphosphanyl)-[1,1′-biphenyl]-2-amine[2]. All reaction solvents were obtained from an Innovative Technology 400-5 Solvent Purification system and stored over 4 Å molecular sieves unless otherwise stated. Pyridine was dried over CaH_2, distilled under dynamic vacuum, and stored under an inert atmosphere over activated 4 Å molecular sieves. Deuterated solvents were obtained from commercially available sources and stored over 4 Å molecular sieves under an inert atmosphere, unless otherwise stated. Acetone-d_6 and toluene-d_8 were purchased in glass ampoules and used as received.

All NMR spectra were obtained using either a 600 or 400 MHz Brüker, or 600 MHz Varian NMR spectrometer at 25 ˚C, unless otherwise indicated. ^{1}H and ^{13}C{^{1}H} spectra were referenced internally to TMS at 0 ppm as follows: benzene-d_6 (^{1}H, 7.16 ppm; ^{13}C{^{1}H}, 128.1 ppm), $CDCl_3$ (^{1}H, 7.26 ppm; ^{13}C{^{1}H} 77.2 ppm), toluene-d_8 (^{1}H, 2.08 ppm, ^{13}C{^{1}H}, 20.4 ppm), acetone-d_6 (^{1}H, 2.05 ppm; ^{13}C{^{1}H}, 205.9 ppm).^{31}P{^{1}H} spectra obtained in deuterated solvents were referenced internally to H_3PO_4 at 0.0 ppm, whereas spectra acquired in non-deuterated solvents were referenced (to H_3PO_4 at 0.0 ppm) by external method to a sample of 85% H_3PO_4. Multiplicities are identified as s (singlet), d (doublet), t (triplet), sept (septet), m (multiplet), or br (broad). Chemical shift assignments were obtained using 1D NMR spectroscopy and 2D heteronuclear and homonuclear NMR spectroscopy (i.e. ^{1}H-^{1}H COSY, ^{1}H-^{13}C HSQC, ^{1}H-^{13}C/^{31}P/^{15}N HMBC). Charge-transfer matrix-assisted laser desorption/ionization (MALDI) mass spectrometry data were collected on an AB Sciex 5800 TOF/TOF mass spectrometer using pyrene as the matrix in a 20:1 molar ratio to metal complex. Samples were spotted on the target plate as solutions in CH_2Cl_2. ESI-MS spectra were acquired on a Thermo Orbitrap Exploris 120 mass spectrometer in positive ion mode. The ion transfer tube temperature was set to 275˚C, with a vaporizer temperature of 300˚C with a positive ion discharge current of 4 μA. Sample solutions were prepared in toluene at a concentration of 1 mg/mL, diluted 100 fold, and injected into the spectrometer with a flow rate of 25 μL/min with a secondary flow of isopropanol at a flow rate of 0.150 mL/min to minimize the fragmentation and charring of the sample. Infrared spectra were collected on solid samples using a PerkinElmer UATR TWO FTIR spectrometer. UV-Visible spectra were collected using an Agilent Technologies Cary 8454 UV-Visible spectrometer.

X-ray absorption spectroscopy. Complexes **2**, **A** and **B** were transferred into glass vials under argon and transported to the Canadian Light Source (CLS, Saskatoon, Canada) in a thermal cup filled with ice gel to avoid potential thermal degradation before XAS measurements. Sample preparation for XAS was done in a glovebox. Pd K-edge XANES and EXAFS spectroscopies of three Pd complexes (**2**, **A**, and **B**) were collected on the HXMA beamline. The beamline energy was calibrated using a

palladium foil as a reference (E_0 = 24,350 eV). The fluorescence yield (FY) spectrum of each sample was recorded by collecting Pd Kα X-ray and normalized to the incident photon flux (I_0). Reference samples Pd metal, $PdCl_2$ and PdS were measured in transmission mode. Pd L_3-edge and P K-edge XANES was collected on the SXRMB beamline. Photon energy was calibrated using red phosphorus as a reference (E_0 = 2,145.5 eV). Both total electron yield (TEY) and partial FY were recorded by measuring the sample current and Pd Lα/P Kα X-ray, respectively, and normalized to the incident photon flux. All XANES and EXAFS spectra were processed using the Athena software (version 0.9.26). Pd K-edge XANES and EXAFS of PdP complexes (**2**, **A**, and **B**) was smoothed with a boxcar width of 5.

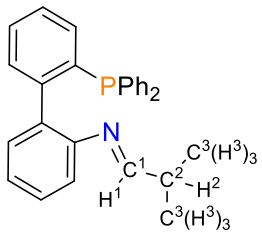

Figure S1. General labelling scheme for carbons and protons of azaallyl arm. This scheme will be used consistently for all compounds used throughout the experimental. In cases where H^3 and C^3 atoms are non-equivalent, H^3 and $H^{3'}$, C^3 and $C^{3'}$ will be used when applicable.

Synthesis of the Tautomeric Mixture of H[L2]a and H[L2]b

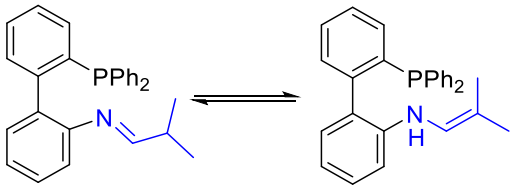

H[L2]a **H[L2]b**

In a glovebox, 2'-(diphenylphosphanyl)-[1,1'-biphenyl]-2-amine (237 mg, 0.671 mmol) was dissolved in toluene (20 mL) and added to a 100 mL Schlenk flask containing a magnetic stir bar and 4 Å molecular sieves. The Schlenk flask was then removed from the glovebox and attached to a Schlenk line. Isobutyraldehyde (0.080 mL, 0.874 mmol) and five drops of formic acid were individually added to the Schlenk flask by a plastic syringe through a septum, and the flask was left to stir for 24 h at room temperature. After 24 h, the solution was filtered through a pad of Celite in a fritted funnel via cannula transfer. The original flask was washed with degassed toluene (3 × 10 mL) and the washings were filtered through the Celite pad. The solvent of the combined filtrates was removed under vacuum at 60 ˚C to afford a viscous yellow oil. **H[L2]** is a mixture of two tautomers: the imine **H[L2]a**, and the enamine **H[L2]b** in a 1:2 ratio, respectively. Yield: 240 mg, 0.589 mmol (88%).

^{1}H NMR (600 MHz, $CDCl_3$): **H[L2]a**: δ = 7.55 (d, *J* = 4.7 Hz, 1H, H^1), 7.47 – 7.04 (m), 6.96 – 6.59 (m), 2.39 (sept. of d, *J* = 4.7 Hz, 1.7 Hz, 1H, H^2), 0.97– 0.89 (m, 6H, H^3). **H[L2]b**: δ = 7.47 – 7.04 (m), 6.96 – 6.59 (m), 6.08 (d, *J* = 10.1 Hz, 1H, H^1), 4.94 (d, *J* = 10.1 Hz, 1H, N*H*), 1.71 (s, 3H, H^3), 1.39 (s,

3H, H^3). $^{31}P\{^1H\}$ NMR (162 MHz ($CDCl_3$): **H[L2]a**: δ = –12.4 (s). **H[L2]b**: δ = –13.3 (s). $^{13}C\{^1H\}$ NMR (151 MHz, $CDCl_3$): **H[L2]a**: δ =171.2 (s, C^1) 150.7 (s), 145.9 (d, J = 30.6 Hz), 138.8 (d, J = 13.6 Hz), 137.3 (d, J = 6.9 Hz), 133.9 (d, J = 5.2 Hz), 133.4 (s) 131.3 (d, J = 4.2 Hz), 130.9 (d, J = 5.3 Hz), 128.6 (s), 128.5 (s), 128.4 (s), 128.3 (s), 128.2 (s) 127.3, (s), 123.8 (s), 119.6 (s), 34.6 (s, C^2), 18.0 (s, C^3). **H[L2]b**: δ = 144.2 (d, J = 30.5 Hz) 141.3 (s), 137.4 (d, J = 7.8 Hz), 137.0 (d, J = 11.7 Hz), 134.3 (s), 134.0 (d, J = 5.9 Hz), 131.0 (d, J = 3.4 Hz), 130.8 (d, J = 4.5 Hz), 129.6 (s), 129.1 (s), 129.8 (d, J = 6.9 Hz), 128.4 (s), 128.3 (s), 126.7 (d, J = 6.9 Hz), 121.3 (s, C^1), 117.3 (s), 110.7 (s), 109.7 (s, C^2) 22.5 (s, C^3), 16.1 (s, C^3). ATR-FTIR (cm^{-1}): ν 3067 (C_{sp}^3 –H, w), 1680 (C=N). ESI MS: *m/z* found: 408.1870, calc: [**H[L2]** + H]$^+$ 408.1881.

Synthesis of K[L2]

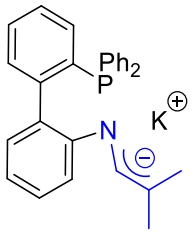

K[L2]

In a glovebox, **H[L2]** (67 mg, 0.164 mmol) was dissolved in anhydrous, stabiliser-free THF (2 mL) and added to a suspension of K[HMDS] (33 mg, 0.164 mmol) in THF (2 mL) in a 20 mL vial. The **H[L2]** solution was added to the K[HMDS] vial with vigorous stirring, and immediately the solution changed colour from pale yellow to light orange, before becoming a dark red upon full addition of **H[L2]**. The reaction solution was left to stir for 0.5 h at room temperature, after which the solvent was removed under vacuum. Pentane (2 mL) was then added, and the suspension was left to stir overnight to solubilize the H[HMDS] by-product. The solvent was removed by pipette, and the precipitate was dried under vacuum to afford **K[L2]** as a yellow-orange powder. NOTE: **K[L2]** is thermally unstable and was stored in the freezer (–20 ˚C). Yield: 55 mg, 0.12 mmol (76%).

^1H NMR (600 MHz, $(CD_3)_2CO$): δ = 7.53 – 7.49 (m, 1H), 7.43 – 7.39 (m, 1H), 7.35-7.30 (m, 6H), 7.29-7.26 (m, 1H) 7.20 – 7.09 (m, 6H), 6.82 (d, J = 8.4 Hz, 1H), 6.71 (d, J = 7.2 Hz, 1H), 6.56 – 6.50 (m, 1H), 6.15 (s, 1H, H^1), 1.66 (s, 3H, H^3), 1.32 (s, 3H, H^3). $^{31}P\{^1H\}$ NMR (243 MHz, $(CD_3)_2CO$): δ = –13.6 (s). $^{13}C\{^1H\}$ NMR (151 MHz, $(CD_3)_2CO$)): δ = 145.0 (d, J_{CP} = 31.5), 141.6 (s), 138.9 (d, J = 14.1 Hz), 137.9 (d, J = 13.5 Hz), 137.8 (d, J = 12.9 Hz), 134.5 (s) 134.1 (d, J = 20.0 Hz,), 134.0 (d, J = 20.0 Hz) , 131.2 (d, J = 5.3 Hz), 131.1 (d, J = 3.0 Hz), 130.1 (s), 129.2 (s), 129.0 (d, J = 10.6 Hz), 128.9 (d, J = 6.04 Hz,), 121.7 (s, C^1), 117.5 (s), 111.0 (s), 108.7 (s, C^2), 22.1 (s, C^3) 15.6 (s, C^3). ATR-FTIR (cm^{-1}): ν 3049 (C_{sp}^3–H, w), 1090 (P–Ar, m). MALDI MS (pyrene) collected in negative ion mode *m/z* found: 406.2, calc. [**L2**]$^-$: 406.2.

Synthesis of the Tautomeric Mixture of PdCl(CH$_3$)(H[L2]a), 1a, and PdCl(CH$_3$)(H[L2]b), 1b

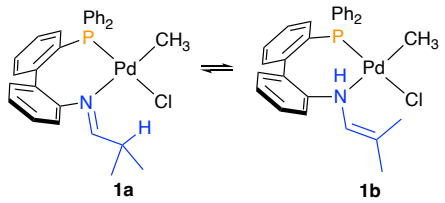

H[L2] (196 mg, 0.48 mmol) was dissolved in DCM (2 mL) and added to a solution of [PdCl(CH$_3$)(COD)] (97.9 mg, 0.4 mmol) and stirred for 2 h at rt. The reaction volume was reduced to 0.5 mL and placed in a freezer at –20 ˚C for 10 min. Cold pentane (6 mL) was added to produce a white precipitate. The solvent was decanted via pipette and the white solid was washed with cold pentane (3 × 4 mL), and the solid was dried under vacuum to yield the mixture of **1a** and **1b** as a white powder. Yield: 160 mg, 59% (0.283 mmol).

^{1}H NMR (600 MHz, CDCl$_3$): **1a**: δ =7.39 – 7.34 (m, 4H), 7.26 – 7.15 (m, 11H), 6.94 – 6.87 (m, 1H), 6.83 – 6.75 (m, 1H), 6.32 (d, *J* = 7.7 Hz, 1H), 3.53 (d of sept, *J* = 1.0 Hz, 6.6 Hz, 1H, *H*^{2}), 1.19 (d, *J* = 6.6 Hz, 3H, *H*^{3}), 0.68 (d, *J* = 6.6 Hz, 3H, *H*^{3}), 0.47 (d, *J* = 3.4 Hz, 3H, Pd-C*H*$_3$). **1b**: 7.63 – 7.52 (m, 4H), 7.52 – 7.40 (m, 8H), 7.33 – 7.26 (m. 2H), 7.10 – 7.03 (m, 1H), 7.01 – 6.95 (m, 1H), 6.64 – 6.52 (m, 1H), 6.13 (dd, *J* = 1.4 Hz, 7.6 Hz, 1H), 5.90 (br, 1H, N-*H*), 1.65 (br, 3H, *H*^{3}), 1.47 (s, 3H, *H*^{3}), 0.60 (d, *J* = 3.6 Hz, 3H, Pd-C*H*$_3$). ^{31}P{^{1}H} NMR (243 MHz, CDCl$_3$): **1a**: δ = 36.2 (s). **1b**: 35.4 (s). ^{13}C{^{1}H} NMR (151 MHz, CDCl$_3$): **1a**: δ = 179.5 (s), 148.6 (s), 35.3 (s), 19.0 (s) 18.5 (s) 0.76 (d, *J* = 2.9 Hz). **1b**: δ = 121.4 (s), 119.7 (s), 22.5 (s), 22.5 (s), 1.26 (d, *J* = 2.7). The following signals cannot be assigned to specifically **1a** or **1b**. 136.0 (d, *J* = 14.0 Hz), 134.2 (d, *J* = 12.5 Hz) 132.5 (s), 132.4 (s), 132.3 (s), 132.3 (s), 132.3 (s), 132.3 (s), 132.2 (s), 132.2 (s,), 131.6 (s), 131.0 (s), 130.9 (d, *J* = 2.3 Hz), 130.8 (d, *J* = 2.3 Hz), 129.8 (s), 129.4 (s), 129.1 (s), 129.0 (s), 128.8 (s), 128.8 (s), 128.7 (s), 128.6 (s), 128.5 (s), 128.4 (s), 128.4 (s), 128.3 (s), 127.4 (d, *J* = 8.2 Hz), 126.4 (s), 125.4 (s), 124.0 (s), 122.5 (s). ATR-FTIR (cm^{-1}): ν 3306 (N-H, w), 1671 (C=N, m). MALDI MS (pyrene) *m/z* found: 337.1, calc: [**H[L2]**-C$_4$H$_8$N]$^{\bullet+}$ 337.1, found: 347.0, calc: [**1**-CH$_3$]$^{\bullet+}$ 347.0. APCI MS *m/z* found: 527.1036, calc: [**Pd(CH$_3$)(L2) –** Cl]$^+$ 527.1072.

Synthesis of Pd(CH$_3$)(L2), 2

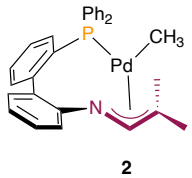

Prior to initiation of the reaction, all components were stored in the glovebox freezer (–20 ˚C) for at least 30 minutes. Separate solutions of **K[L2]** (50 mg, 0.112 mmol) and [PdCl(CH$_3$)(COD)] (27 mg, 0.102 mmol) were prepared in cold THF (2 mL each) in two separate 20 mL vials. The **K[L2]** solution was added dropwise to the stirring solution of [PdCl(CH$_3$)(COD)] resulting in an immediate colour

change from white to orange. The orange solution was stirred for 5 min, and the reaction was filtered through a pad of Celite into a 20 mL vial. The reaction vial was rinsed with THF (0.5 mL portions), and the rinses were passed through the Celite pad until the rinses were no longer yellow. The rinses were filtered, and the filtrates were combined. The solvent of the filtrate was removed under vacuum to give a red residue. The residue was dissolved in Benzene (1 mL) and filtered through a new Celite pad, into a 20 mL vial, washing with Benzene (0.5 mL portions) until the rinses were colourless. The resulting filtrate was concentrated down to *ca.* 0.5 mL, yielding a red residue. Cold Pentane (5 mL) was added to the residue and left in the freezer overnight. The next day, the solvent was decanted, and the vial was dried to yield a dark red-orange solid. NOTE: **2** is thermally unstable and was stored in the freezer (–20 ˚C). Yield: 35 mg, 0.066 mmol (70%).

^{1}H NMR (600 MHz, C_6D_6): δ = 7.57 – 7.50 (m, 4H), 7.09 – 6.95 (m, 7H), 6.92 (m, 1H), 6.88 (s, 1H, *H*^{1}), 6.80 – 6.76 (m, 4H), 6.65 – 6.60 (m, 1H), 6.46 (d, *J* = 7.3 Hz, 1H), 1.82 (d, *J* = 3.8 Hz, 3H, *H*^{3}), 1.72 (d, *J* = 6.9 Hz, 3H, *H*^{3}), 0.52 (d, *J* = 3.6 Hz, 3H, Pd-C*H*$_3$). ^{31}P{^{1}H} NMR (243 MHz, C_6D_6): δ = 25.8 (s, ArPh$_2$*P*-Pd) ^{13}C{^{1}H} NMR (151 MHz, C_6D_6): δ = 153.1 (s), 148.1 (s), 136.2 (d, *J* = 14.1 Hz), 135.4 (d, *J* = 12.2 Hz), 134.7 (d, *J* = 7.0 Hz), 133.0 (s), 132.7 (s), 131.1 (s), 131.0 (d, *J* = 7.6 Hz), 130.6 (d, *J* = 18.0 Hz), 129.7 (d, *J* = 4.7 Hz, *C*^{1}), 128.8 (s), 128.7 (d, *J* = 10.1 Hz), 128.4 (s), 126.6 (d, *J* = 7.0 Hz,), 121.9 (s), 113.9 (s), 88.7 (d, *J* = 28.2 Hz, *C*^{2}), 21.8 (d, *J* = 4.1 Hz, *C*^{3}), 20.9 (d, *J* = 5.0 Hz, *C*^{3}), –1.3 (d, *J* = 11.8 Hz Pd-*C*H$_3$). ATR-FTIR (cm^{-1}): ν 2957 (C_{sp^2} –H, w), 1098 (P– Aryl, m). MALDI MS (pyrene) *m/z* found: 406.1, calc: [**L2**]$^{\bullet+}$ 406.2, found: 512.1, calc: [**2**- CH_3]$^{\bullet+}$ 512.1. APCI MS *m/z*: found 528.1072, calc: [**2** + H]$^{+}$ 528.1066

II – Reactivity Studies: Procedures and Spectra

Reaction of 2 with Pyridine. In a glovebox, a solution of **2** (10 mg, 0.01 mmol) dissolved in C_6D_6 (0.5 mL) was prepared in a 4 mL vial. One equivalent of pyridine was added, and the solution was transferred to an NMR tube, where the sample was analyzed by $^{31}P\{^1H\}$ NMR spectroscopy. This procedure was repeated for pyridine additions of 1, 2, 3, 4, 5, and 10 equiv were made. This reaction was also conducted with **2**, dissolved in a solution of pyridine.

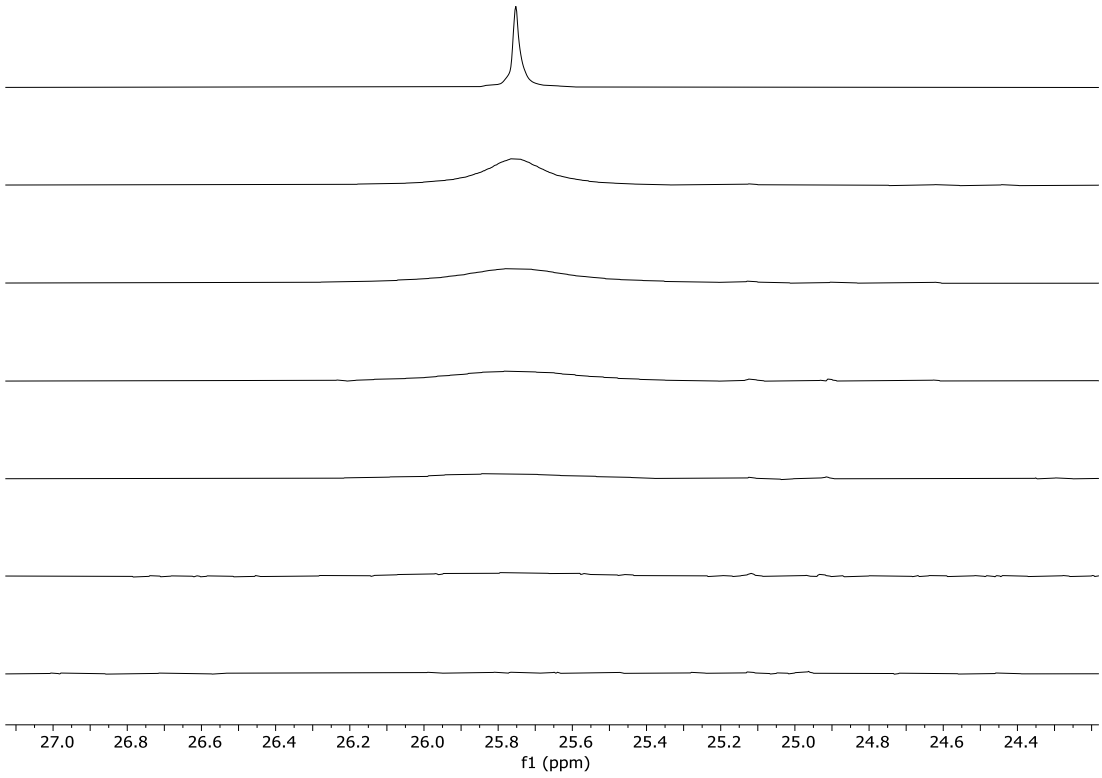

Figure S2. $^{31}P\{^1H\}$ NMR stack plot (243 MHz) of the reaction of **2** with pyridine at rt after ca. 10 min. From top to bottom: **2**, **2** and 1 equiv pyridine, **2** and 2 equiv pyridine, **2** and 3 equiv pyridine, **2** and 4 equiv pyridine, **2** and 5 equiv pyridine, **2** and 10 equiv pyridine in C_6D_6.

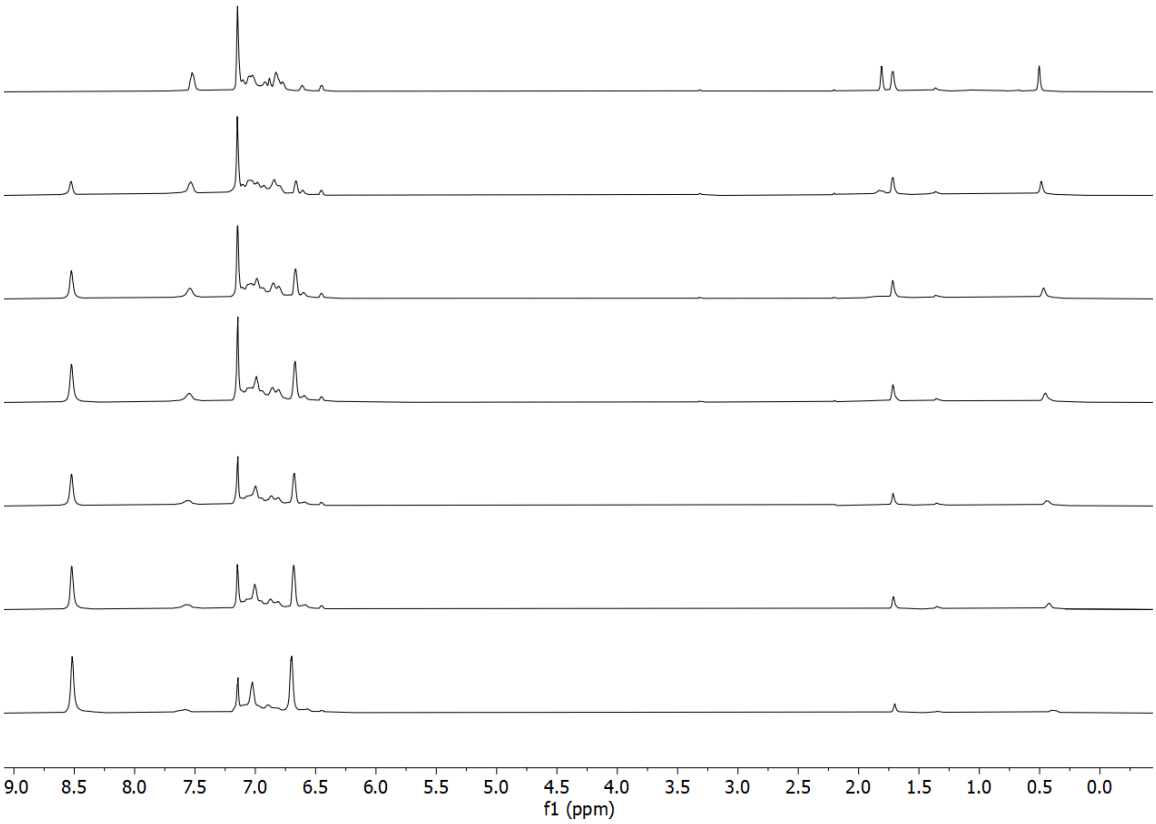

Figure S3. ^{1}H NMR stack plot (600 MHz) of the reaction of **2** with pyridine at rt after ca. 10 min. From top to bottom: **2**, **2** and 1 equiv pyridine, **2** and 2 equiv pyridine, **2** and 3 equiv pyridine, **2** and 4 equiv pyridine, **2** and 5 equiv pyridine, **2** and 10 equiv pyridine in C_6D_6.

Evans Method Analysis: In a glovebox, a solution of **2** (10 mg, 0.02 mmol) was dissolved in 0.5 mL of C_6D_6 in a 20 mL vial. To this vial, 10 equiv pyridine-d_5 was added and the solution was transferred to an NMR tube containing a capillary filled with C_6D_6 + 10 equiv of pyr-d_5. A ^{1}H NMR spectrum was acquired 10 minutes after pyridine-d_5 addition, in which a difference in chemical shift of 0.01 ppm was observed between signals for residual C_6H_6 in the sample solution and from the capillary solvent. To confirm the more downfield signal was due to the capillary sample, the capillary was removed, and a second ^{1}H NMR spectrum was acquired. μ_{eff} was determined to be 0.42 B.M, which is much lower than the expected values for 1 and 2 unpaired electrons of 1.73 and 2.83 B.M., respectively. Thus, the difference in chemical shift between the residual C_6H_6 signals for the sample and capillary are due to the different solvent compositions.

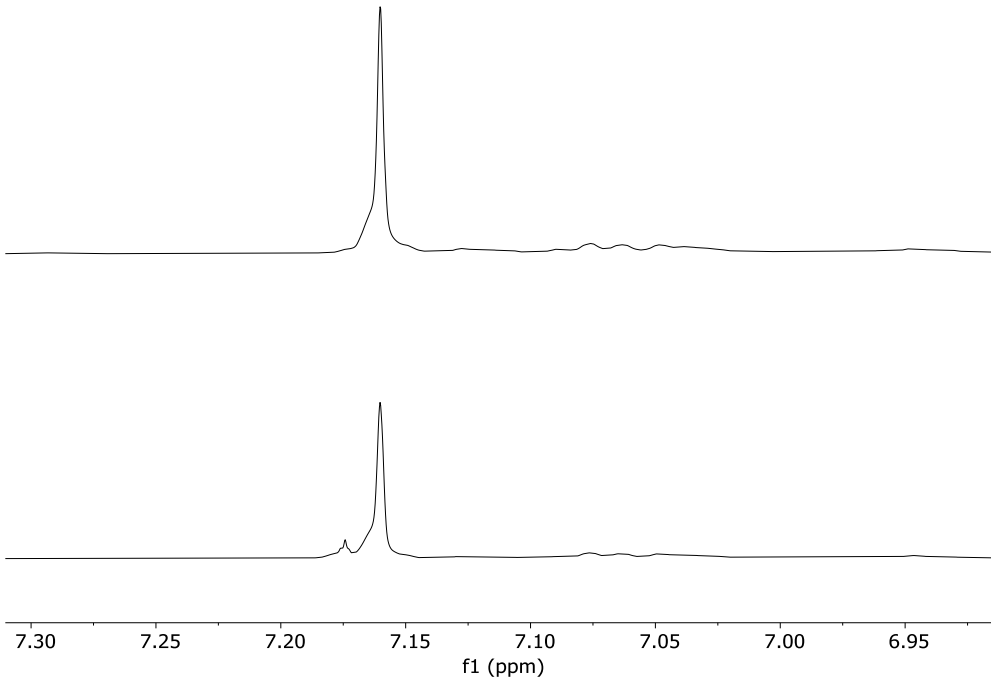

Figure S4. ^{1}H NMR stack plot (600 MHz, C_6D_6) for Evans' method analysis between **2** and pyr-d_5. Top: Reaction mixture with no internal standard. Bottom: Reaction mixture with internal standard of C_6D_6 + pyr-d_5.

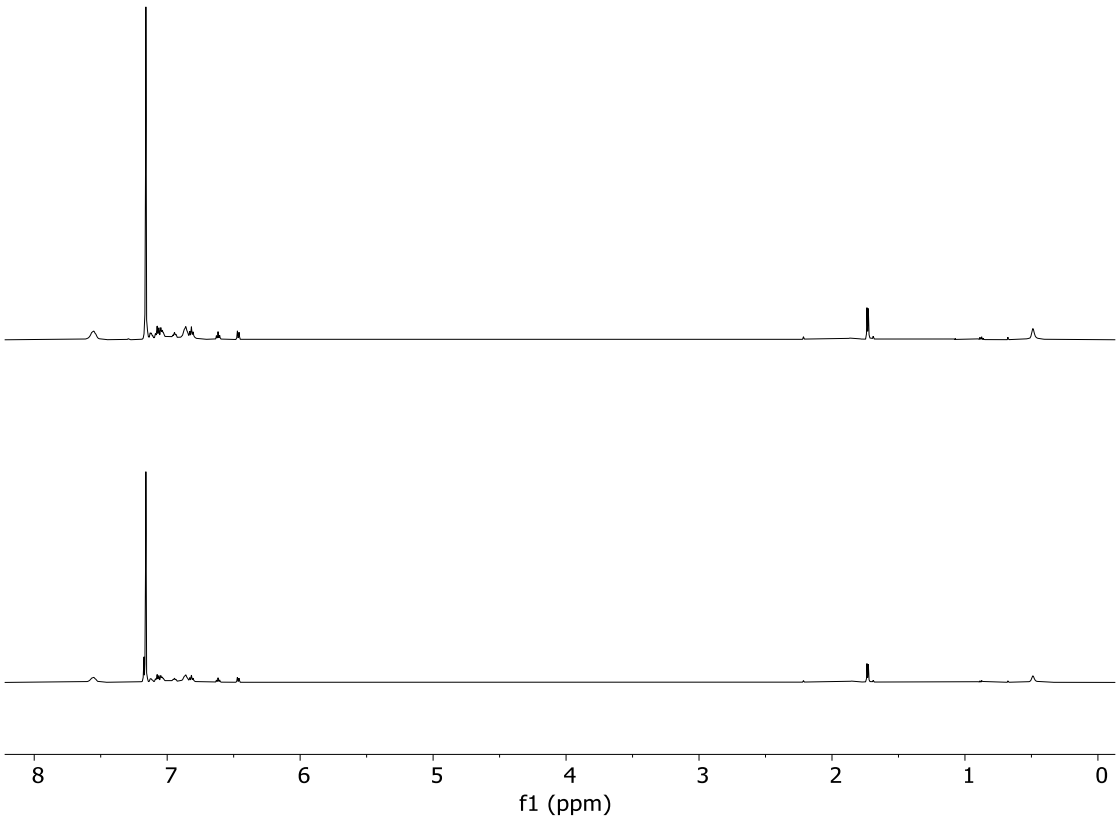

Figure S5. Full ^{1}H NMR stack plot (600 MHz, C_6D_6) for Evans' method analysis between **2** and pyr-d_5. Top: Reaction mixture with no internal standard. Bottom: Reaction mixture with internal standard of C_6D_6 + pyr-d_5.

General Procedure for $B(C_6F_5)_3$ Addition

In a glovebox, a 0.375 mM stock solution of pyridine in C_6D_6 was prepared in a 4 mL vial. In a separate 4 mL vial, a solution of **2** (10 mg, 0.020 mmol) dissolved in the pyridine/C_6D_6 stock solution (1 mL) was prepared. 40 equivalents of $B(C_6F_5)_3$ (100 mg, 0.76 mmol) were dissolved in the solution of **2**, pyridine, and C_6D_6. The solution was transferred to an NMR tube, where it was analyzed by ^{1}H, $^{31}P\{^{1}H\}$, $^{19}F\{^{1}H\}$, and ^{11}B NMR spectroscopies

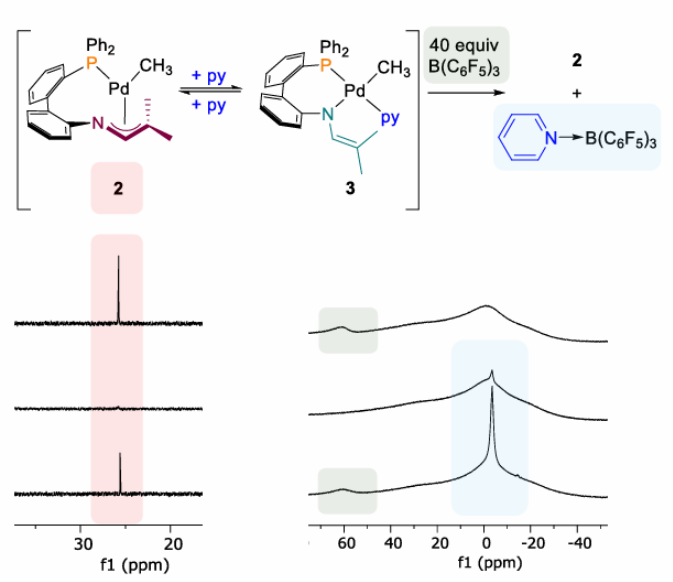

Figure S6. Left: $^{31}P\{^{1}H\}$ NMR stack plot (162 MHz, C_6D_6). From top to bottom: **2**, **2** + 1 equiv. of pyridine, and **2** + 1 equiv. of pyridine + 40 equiv. of $B(C_6F_5)_3$. Right: $^{11}B\{^{1}H\}$ NMR (128 MHz, C_6D_6). From top to bottom, $B(C_6F_5)_3$, $B(C_6F_5)_3$ + pyridine, 1:1:40 **2**, pyridine, and $B(C_6F_5)_3$. $^{11}B\{^{1}H\}$ NMR spectra were collected on samples in borosilicate glass, which is observed as a broad signal that perturbs the baseline of the spectra.

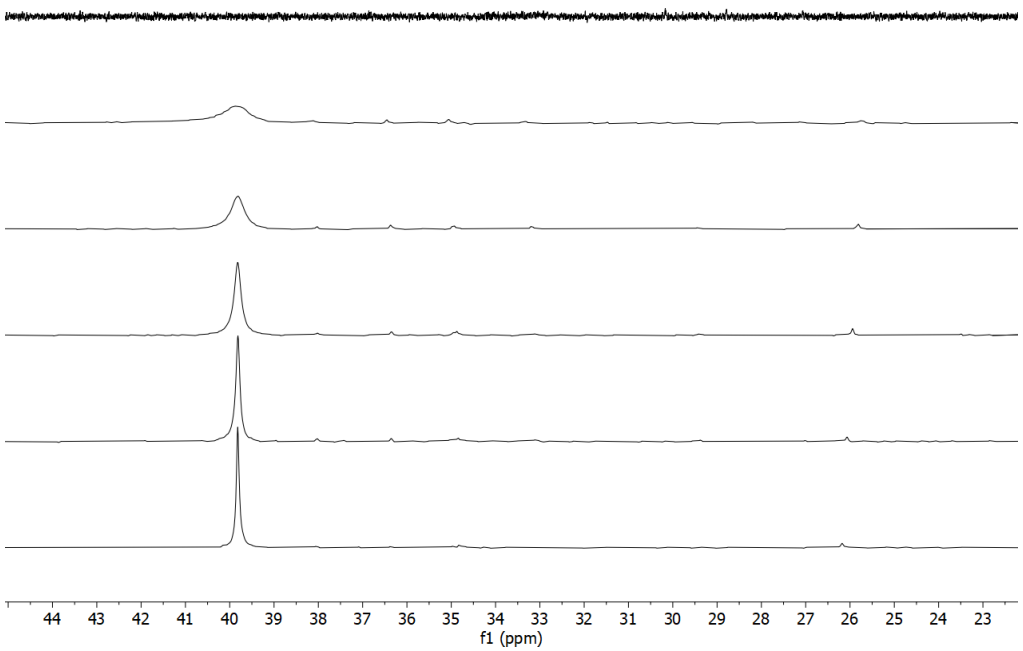

Figure S7. Variable temperature $^{31}P\{^{1}H\}$ NMR spectra (243 MHz) of **2** dissolved in pyr-d_5. From top to bottom: 25, 10, 0, –10, –20, and –30 °C.

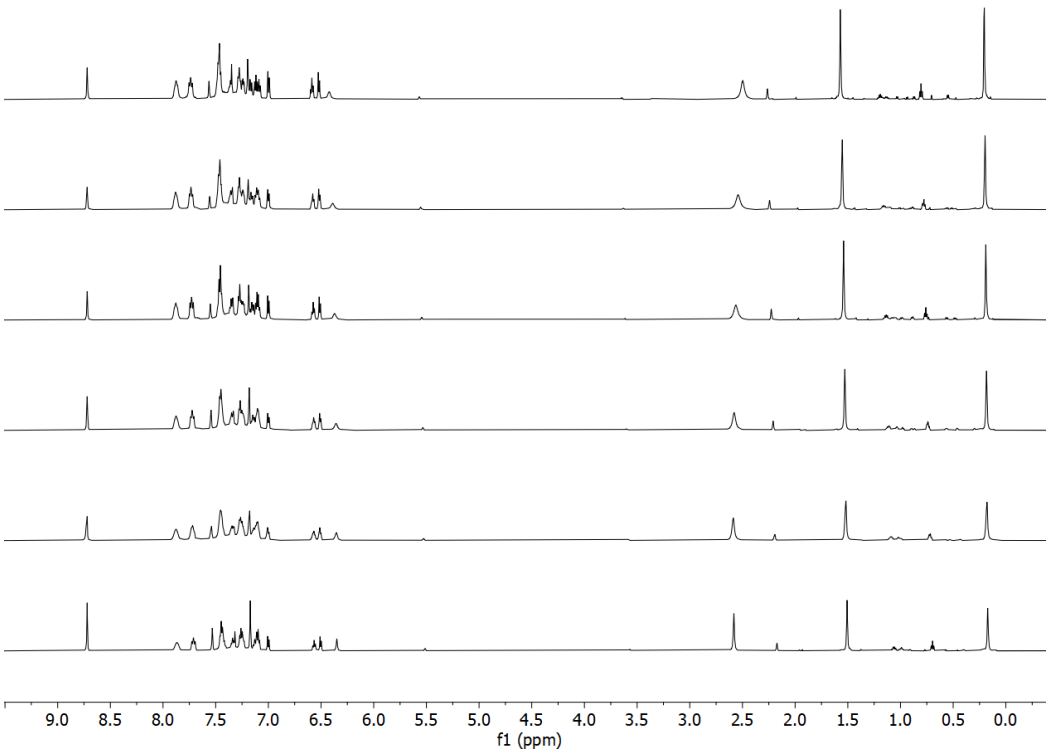

Figure S8. Variable temperature ^{1}H NMR spectra (600 MHz) of **2** dissolved in pyr-d_5. From top to bottom: 25, 10, 0, –10, –20, and –30 °C.

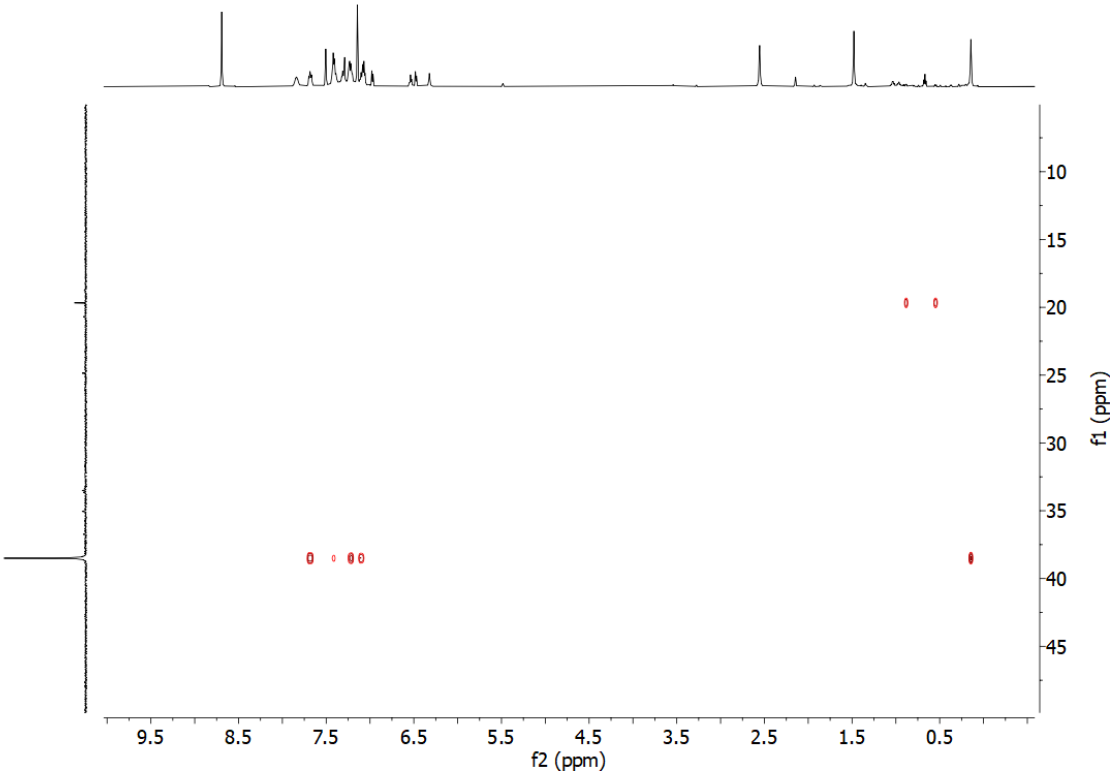

Figure S9. ^{1}H-^{31}P HMBC NMR spectrum (600 MHz) of **2** dissolved in pyridine-d_5, collected at –30 °C.

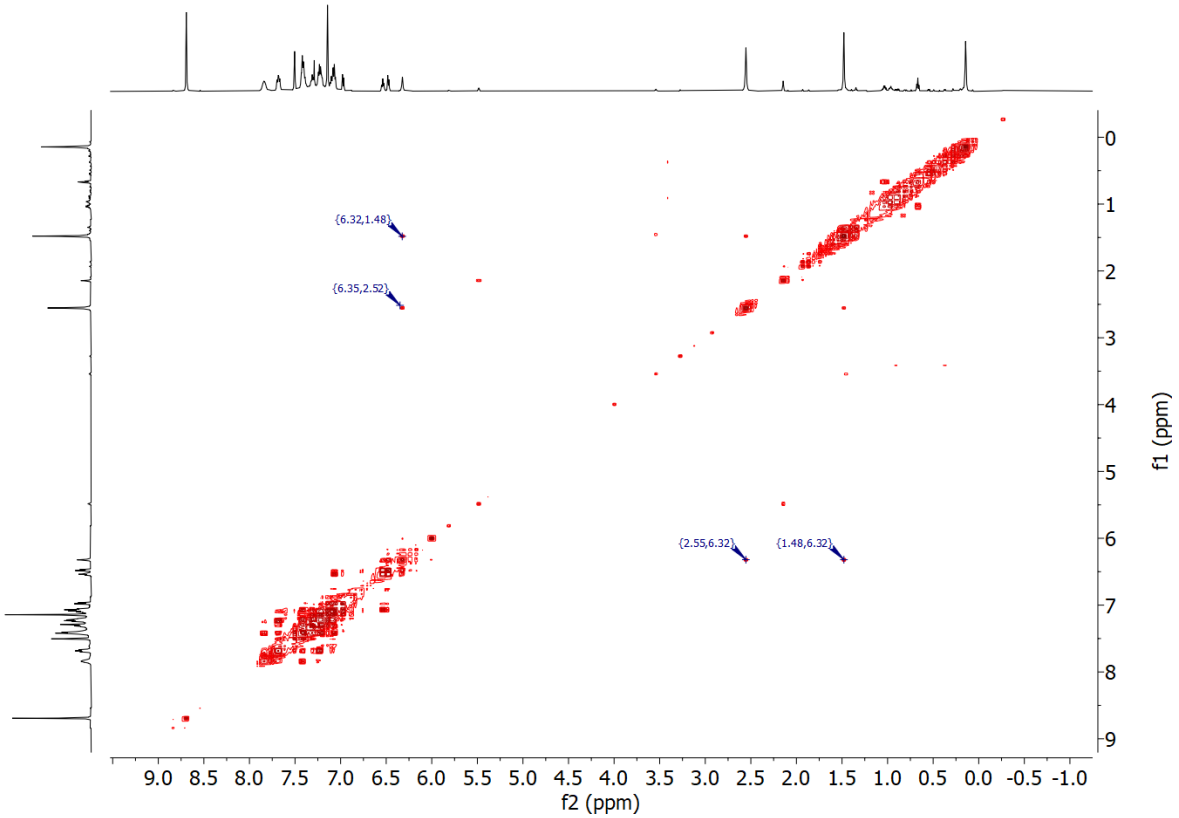

Figure S10. ^{1}H-^{1}H COSY NMR spectrum (600 MHz) of **2** dissolved in pyridine-d_5, collected at –30 °C. Selected signals indicate correlations between H^1 and H^3/$H^{3'}$.

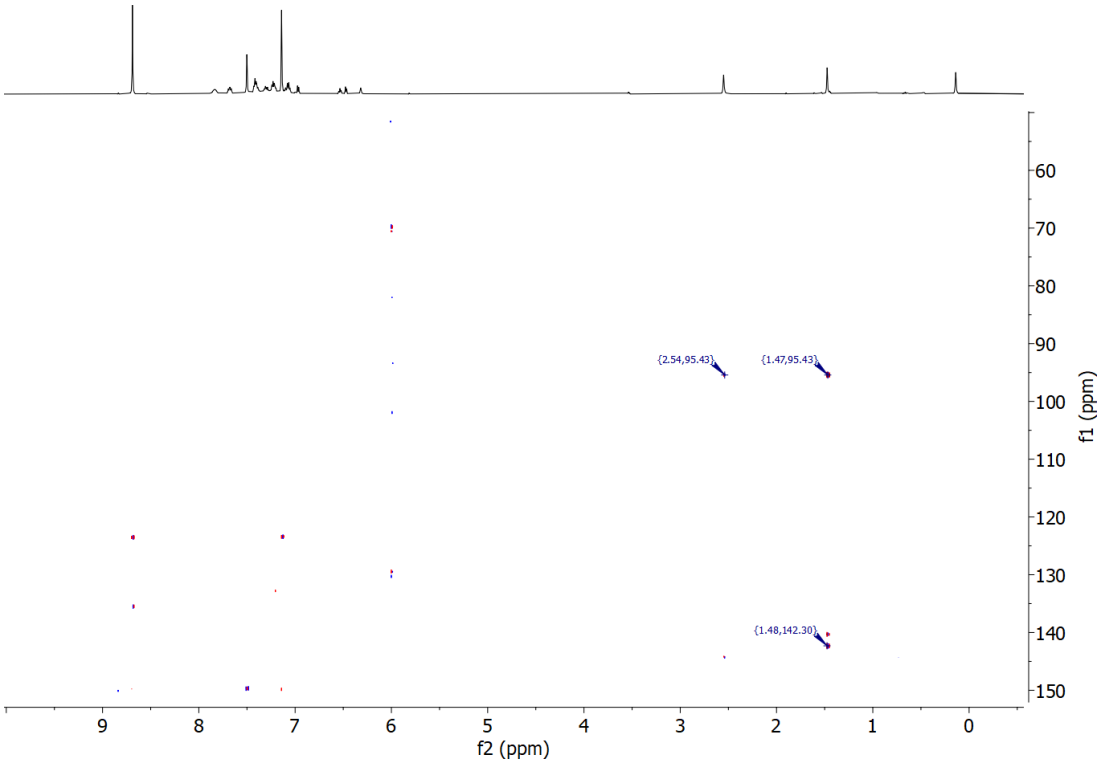

Figure S11. ^{1}H-^{13}C HMBC NMR spectrum (600 MHz) of **2** dissolved in pyridine-d_5, collected at –30 °C. Selected signals indicate correlation between H^3/$H^{3'}$ and C^2 and C^1.

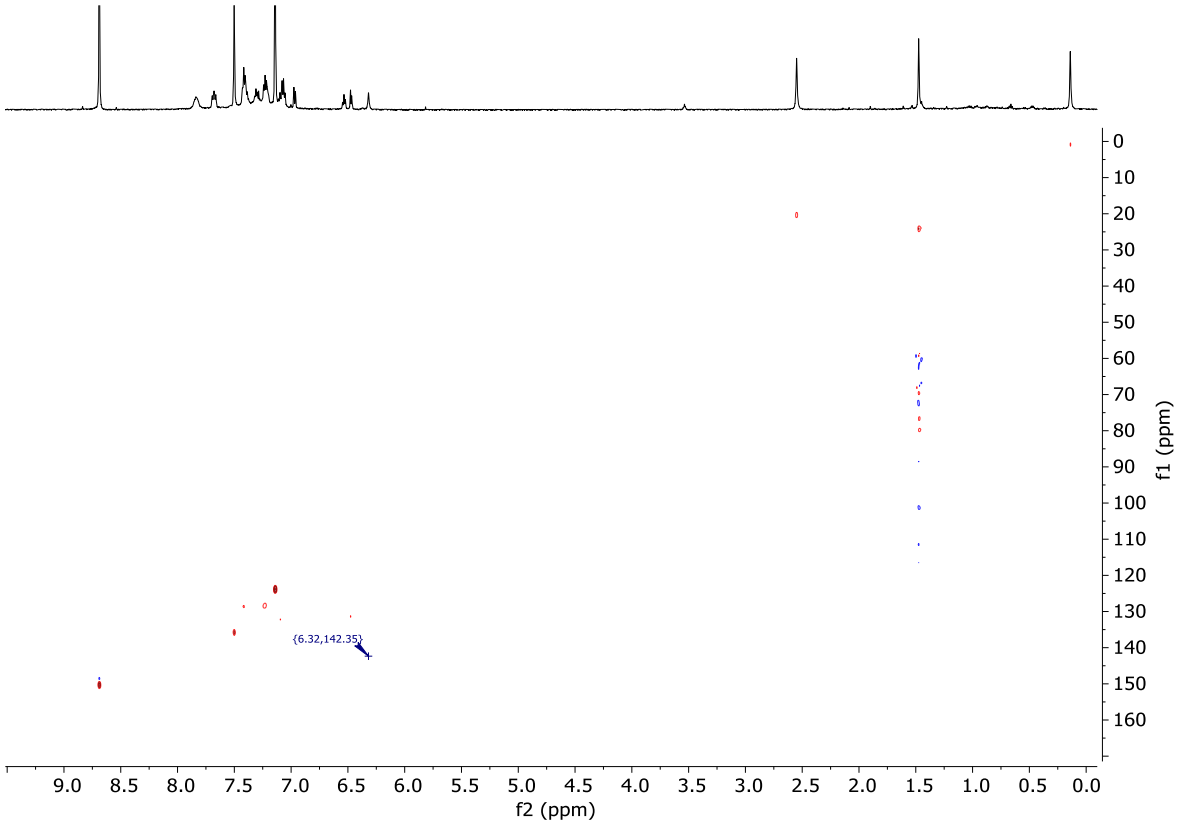

Figure S12. ^{1}H-^{13}C HSQC NMR spectrum (600 MHz) of **2** dissolved in pyridine-d_5, collected at –30 °C. Selected signal indicates assignment of C^1.

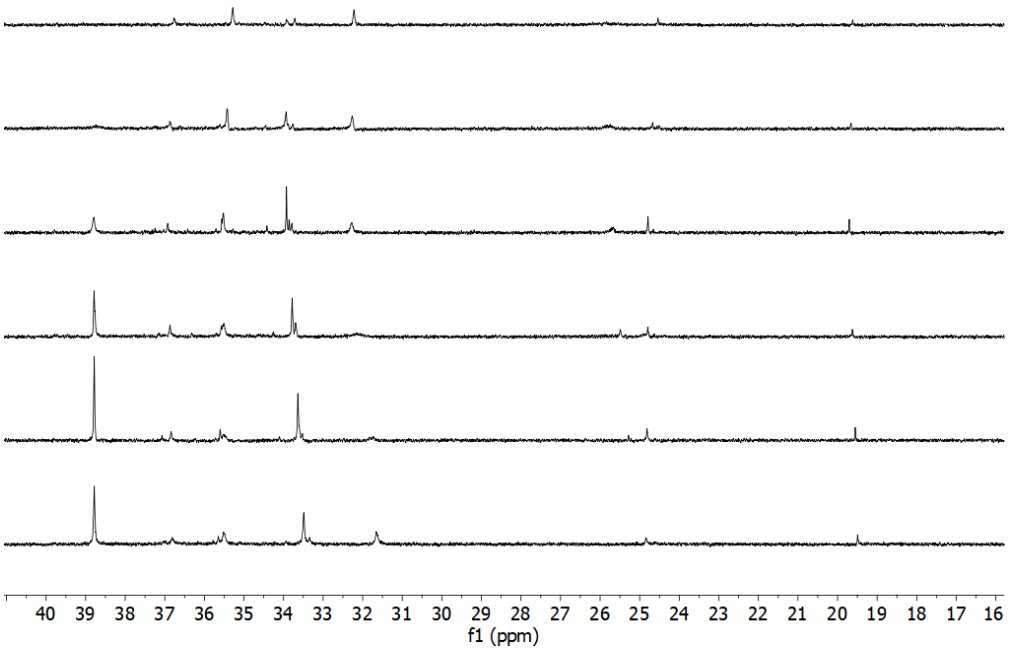

Figure S13. Variable temperature $^{31}P\{^{1}H\}$ NMR spectra (243 MHz, toluene-d_8) stack plot of **2** and 4 equiv pyridine. From top to bottom: 25, 10, 0, –10, –20, –30 °C. There are minor unidentified impurities observed in the $^{31}P\{^{1}H\}$ NMR spectrum for the sample of **2** used for these experiments that account for 6% of the sample (amount determined by relative integration of signals of impurities to signal for **2**).

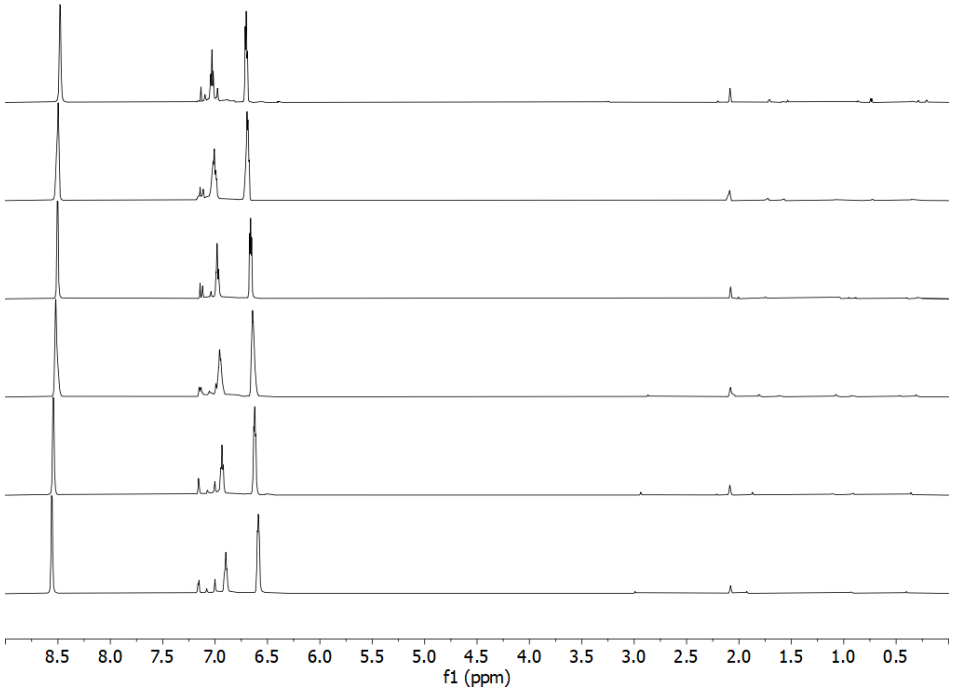

Figure S14. Variable temperature ^{1}H NMR spectra (243 MHz, toluene-d_8) stack plot of **2** and 4 equiv pyridine. From top to bottom: 25, 10, 0, –10, –20, –30 °C. There are minor unidentified impurities observed in the $^{31}P\{^{1}H\}$ NMR spectrum for the sample of **2** used for these experiments that account for 6% of the sample (amount determined by relative integration of signals of impurities to signal for **2**).

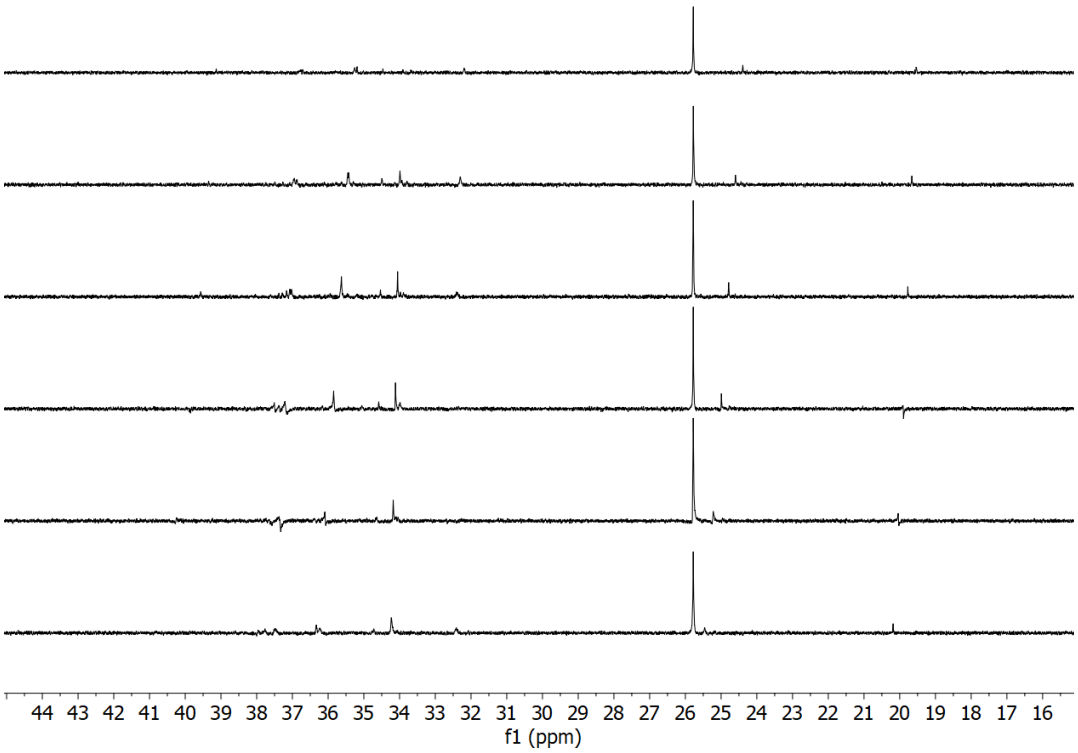

Figure S15. Variable temperature $^{31}P\{^{1}H\}$ NMR spectra (243 MHz, toluene-d_8) stack plot of **2**. From top to bottom: 25, 0, –20, –40, –60, –80 °C. There are minor unidentified impurities observed in the $^{31}P\{^{1}H\}$ NMR spectrum for the sample of **2** used for these experiments that account for 6% of the sample (amount determined by relative integration of signals of impurities to signal for **2**).

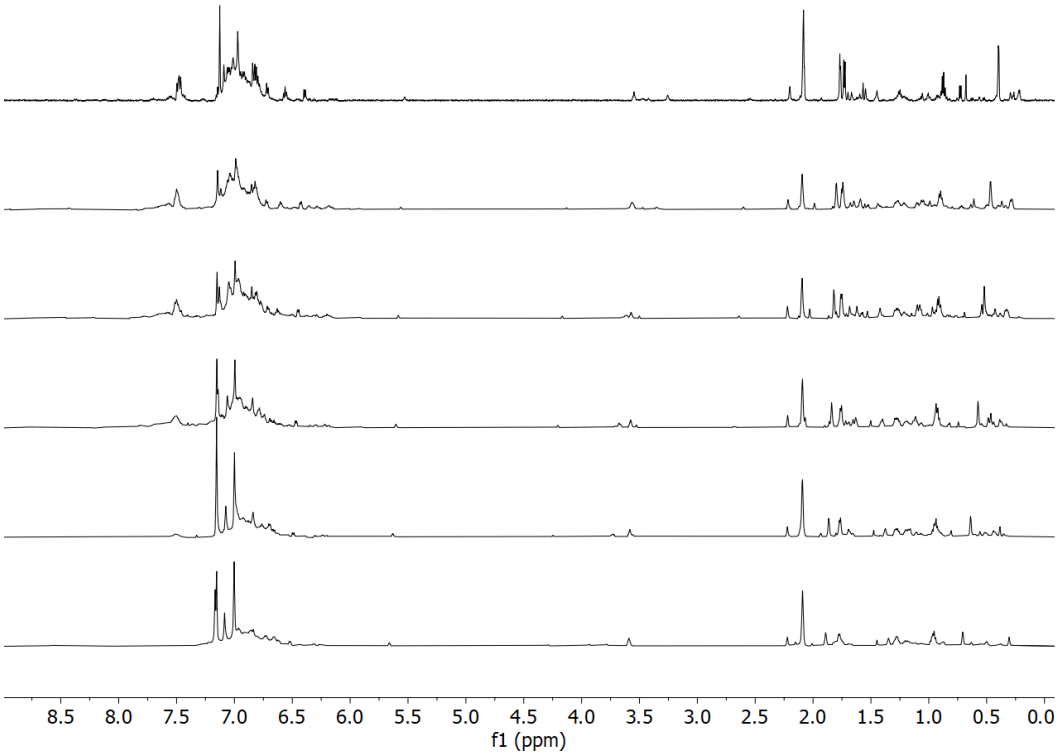

Figure S16. Variable temperature ^{1}H NMR spectra (600 MHz, toluene-d_8) stack plot of **2**. From top to bottom: 25, 0, –20, –40, –60, –80 °C. There are minor unidentified impurities observed in the ^{31}P{^{1}H} NMR spectrum for the sample of **2** used for these experiments that account for 6% of the sample (amount determined by relative integration of signals of impurities to signal for **2**).

III – NMR Spectra

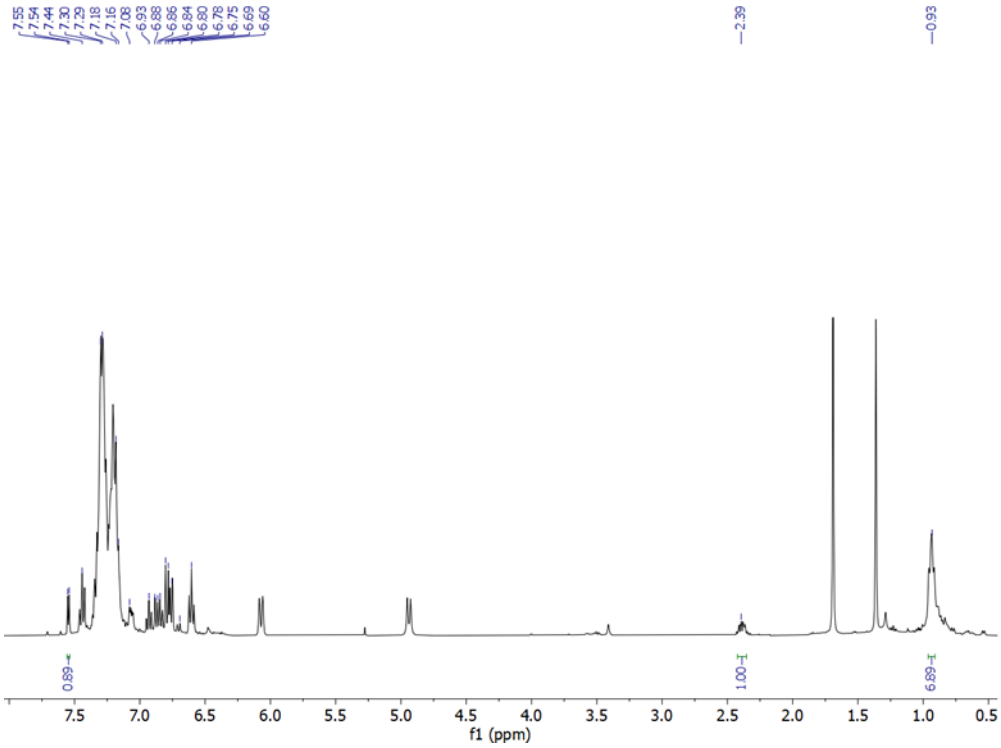

Figure S17. ^{1}H NMR spectrum (400 MHz, $CDCl_3$) of the equilibrium mixture (1:1.7) of $Ph_2P(o\text{-}C_6H_4)(o\text{-}C_6H_4)NCH(i\text{-}Pr)$, **H[L2]a** and $Ph_2P(o\text{-}C_6H_4)(o\text{-}C_6H_4)NHCHC(CH_3)_2$, **H[L2]b**. Selected signals with labelled chemical shifts and integrals correspond to tautomer **H[L2]a**.

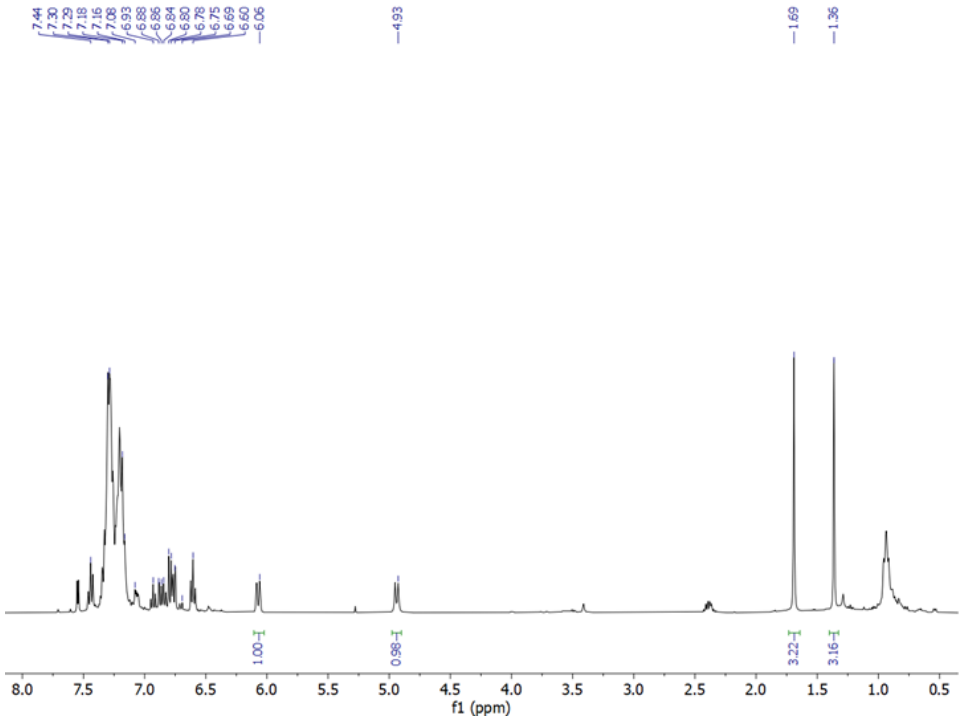

Figure S18. ^{1}H NMR spectrum (400 MHz, $CDCl_3$) of the equilibrium mixture (1:1.7) of $Ph_2P(o\text{-}C_6H_4)(o\text{-}C_6H_4)NCH(i\text{-}Pr)$, **H[L2]a** and $Ph_2P(o\text{-}C_6H_4)(o\text{-}C_6H_4)NHCHC(CH_3)_2$, **H[L2]b**. Selected signals with labelled chemical shifts and integrals correspond to tautomer **H[L2]b**.

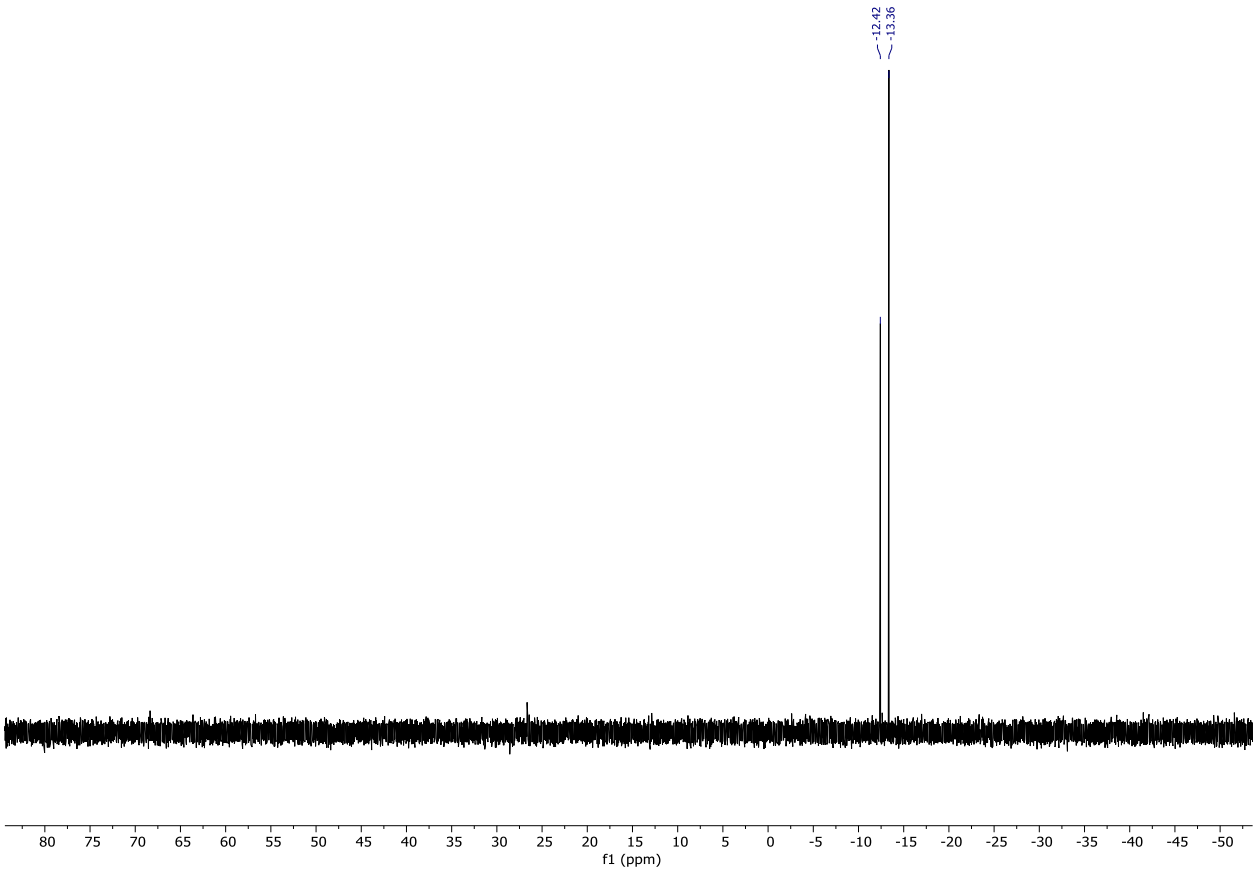

Figure S19. $^{31}P\{^{1}H\}$ NMR spectrum (243 MHz, $CDCl_3$) of the equilibrium mixture (1:1.7) of $Ph_2P(o\text{-}C_6H_4)(o\text{-}C_6H_4)NCH(i\text{-}Pr)$, **H[L2]a** and $Ph_2P(o\text{-}C_6H_4)(o\text{-}C_6H_4)NHCHC(CH_3)_2$, **H[L2]b**.

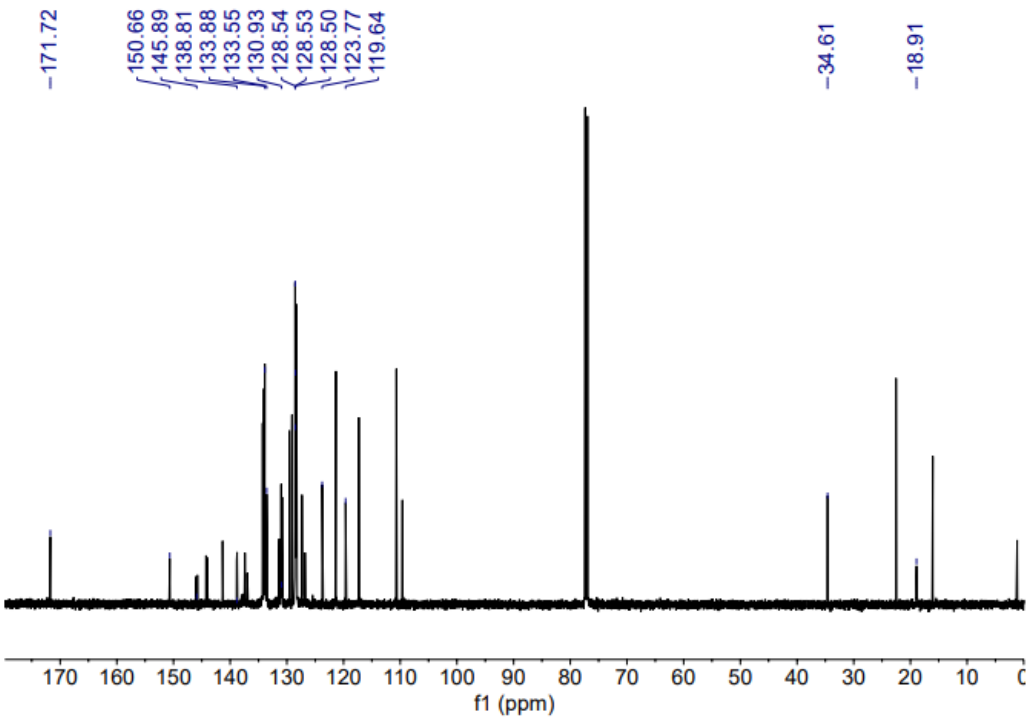

Figure S20. $^{13}C\{^{1}H\}$ NMR spectrum (151 MHz, $CDCl_3$) of the equilibrium mixture (1:1.7) of $Ph_2P(o\text{-}C_6H_4)(o\text{-}C_6H_4)NCH(i\text{-}Pr)$, **H[L2]a** and $Ph_2P(o\text{-}C_6H_4)(o\text{-}C_6H_4)NHCHC(CH_3)_2$), **H[L2]b**. Selected picked peaks correspond to tautomer **H[L2]a**.

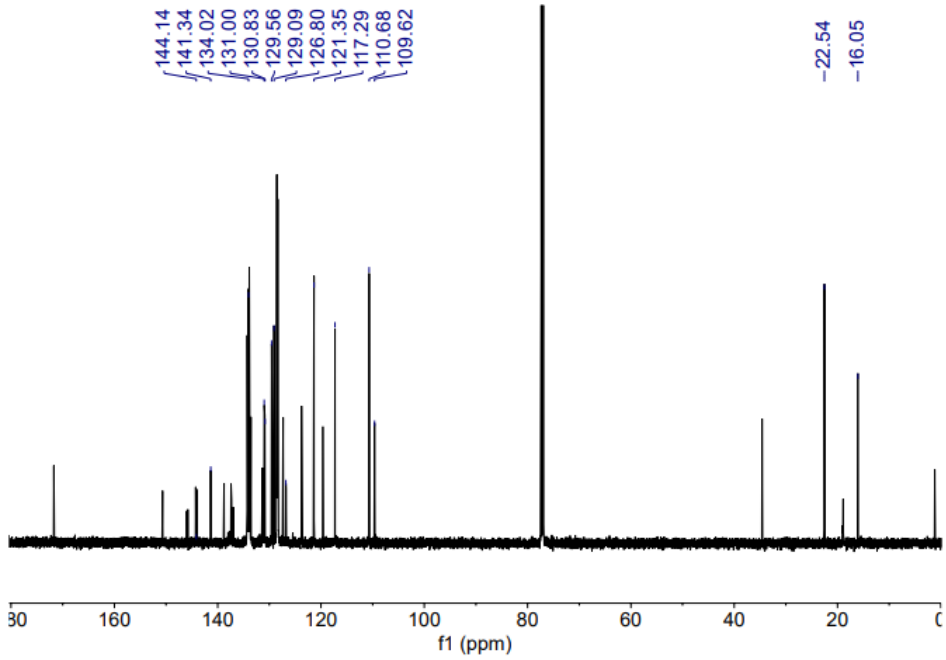

Figure S21. $^{13}C\{^{1}H\}$ NMR spectrum (151 MHz, $CDCl_3$) of the equilibrium mixture (1:1.7) of $Ph_2P(o\text{-}C_6H_4)(o\text{-}C_6H_4)NCH(i\text{-}Pr)$, **H[L2]a** and $Ph_2P(o\text{-}C_6H_4)(o\text{-}C_6H_4)NHCHC(CH_3)_2$), **H[L2]b**. Selected picked peaks correspond to tautomer **H[L2]b**.

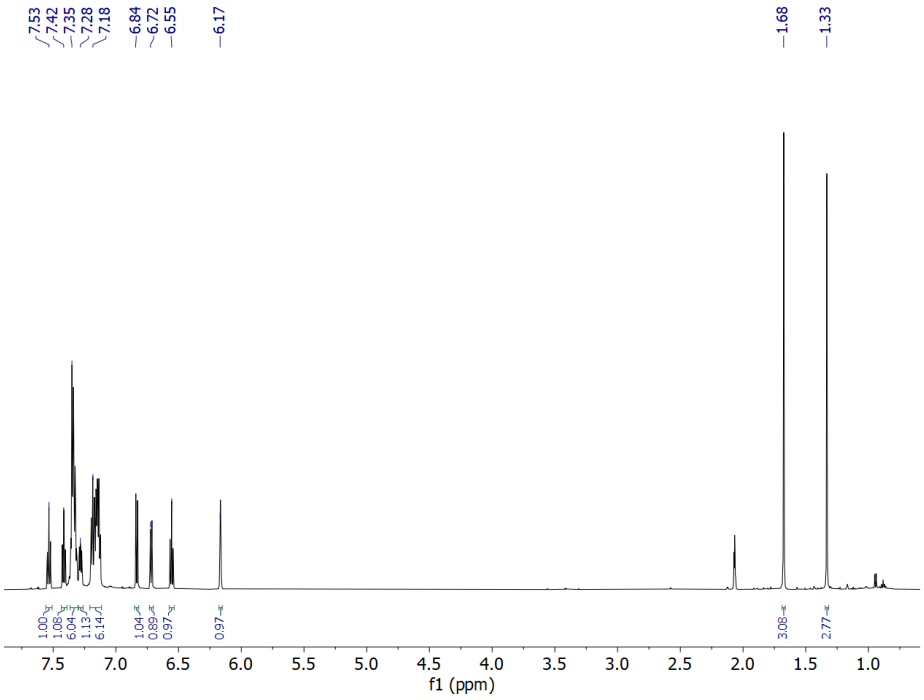

Figure S22. ^{1}H NMR spectrum (600 MHz, $(CD_3)_2CO$) of K[$Ph_2P(o\text{-}C_6H_4)(o\text{-}C_6H_4)NCHC(CH_3)_2$], **K[L2]**.

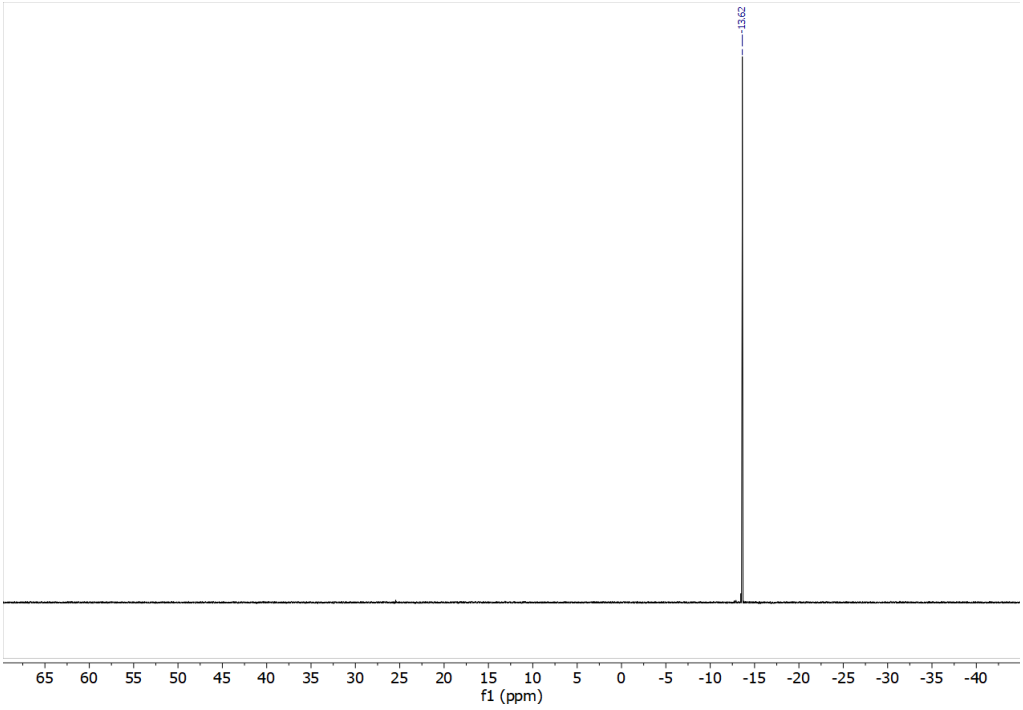

Figure S23. $^{31}P\{^{1}H\}$ NMR spectrum (243 MHz, $(CD_3)_2CO$) of K[$Ph_2P(o\text{-}C_6H_4)(o\text{-}C_6H_4)NCHC(CH_3)_2$], **K[L2]**.

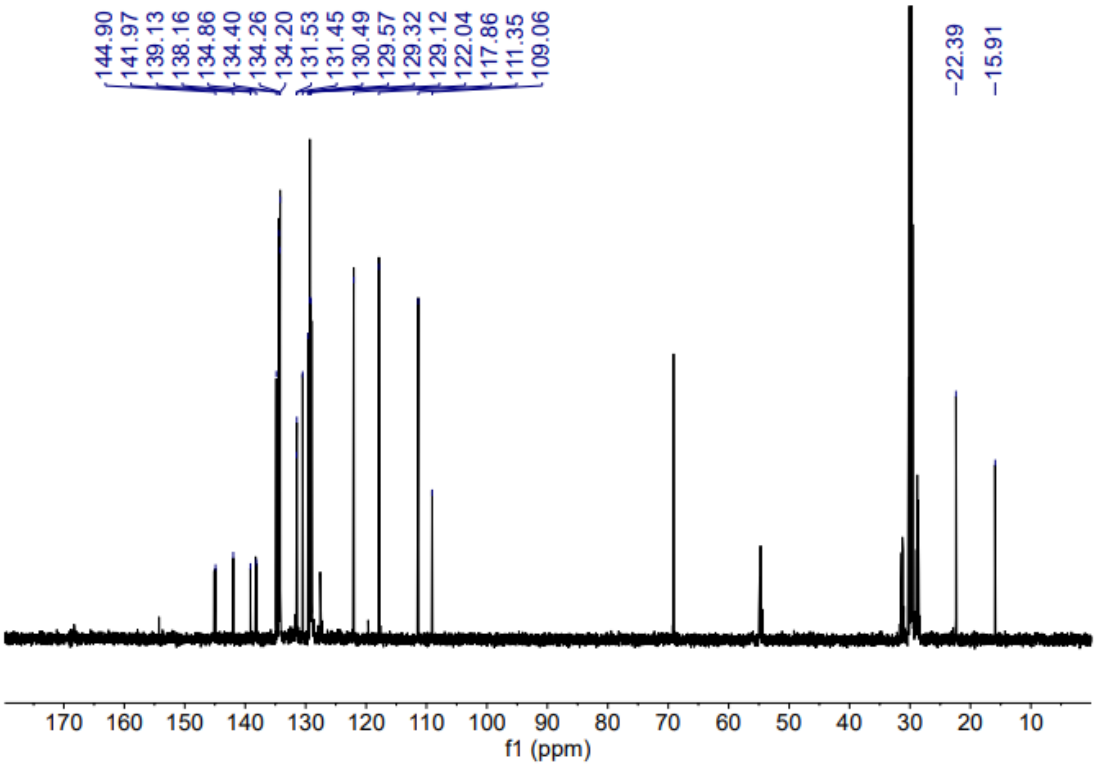

Figure S24. $^{13}C\{^{1}H\}$ NMR spectrum (151 MHz, $(CD_3)_2CO$) of K[$Ph_2P(o\text{-}C_6H_4)(o\text{-}C_6H_4)NCHC(CH_3)_2$], **K[L2]**.

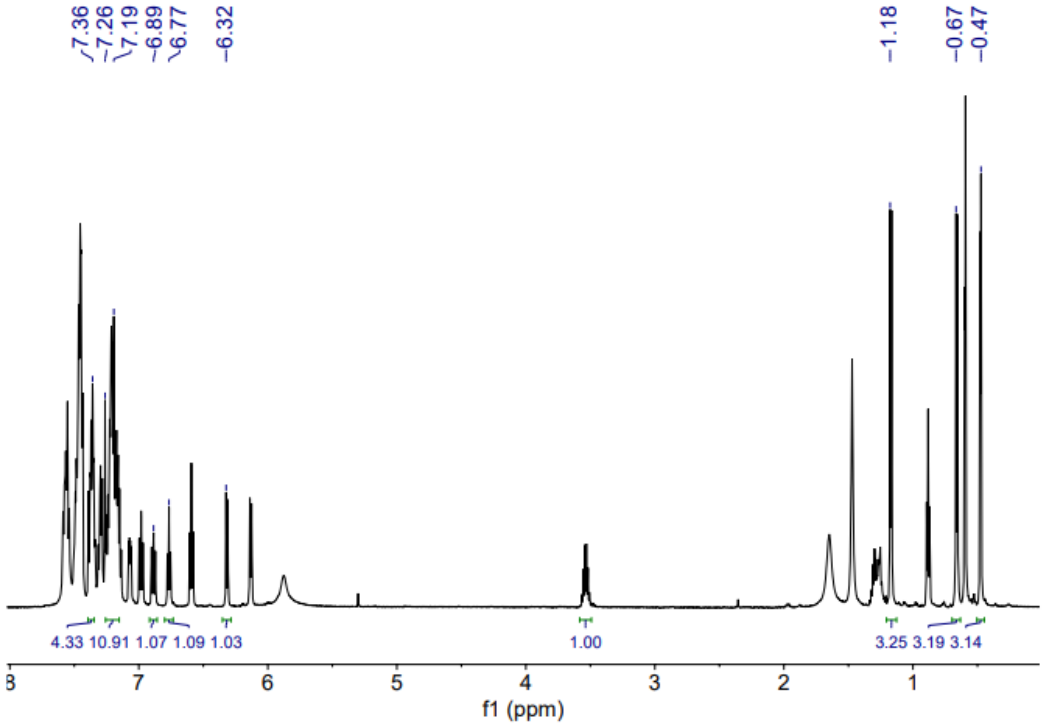

Figure S25. ^{1}H NMR spectrum (600 MHz, $CDCl_3$) of the equilibrium mixture (1:1) of [$PdCl(CH_3)$(**H[L2]a**)], **1a**, and [$PdCl(CH_3)$(**H[L2]b**)], **1b**. Selected signals with labelled chemical shifts and integrals correspond to tautomer **1a**.

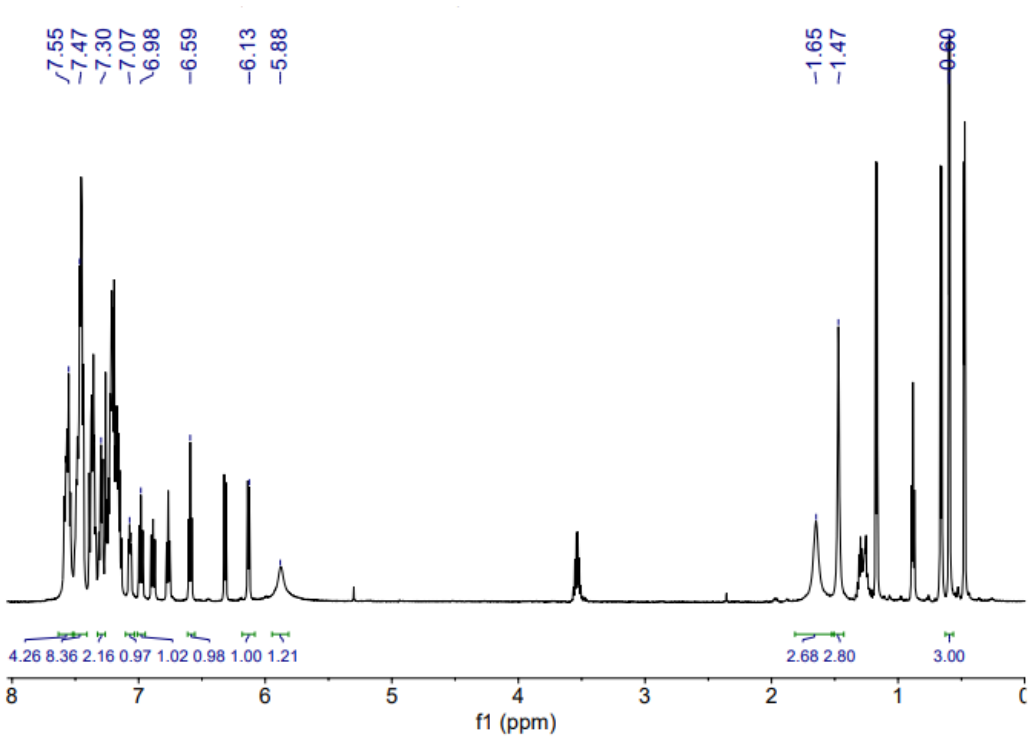

Figure S26. ^{1}H NMR spectrum (600 MHz, $CDCl_3$) of the equilibrium mixture (1:1) of [PdCl(CH_3)(**H[L2]a**)], **1a**, and [PdCl(CH_3)(**H[L2]b**)], **1b**. Selected signals with labelled chemical shifts and integrals correspond to tautomer **1b**.

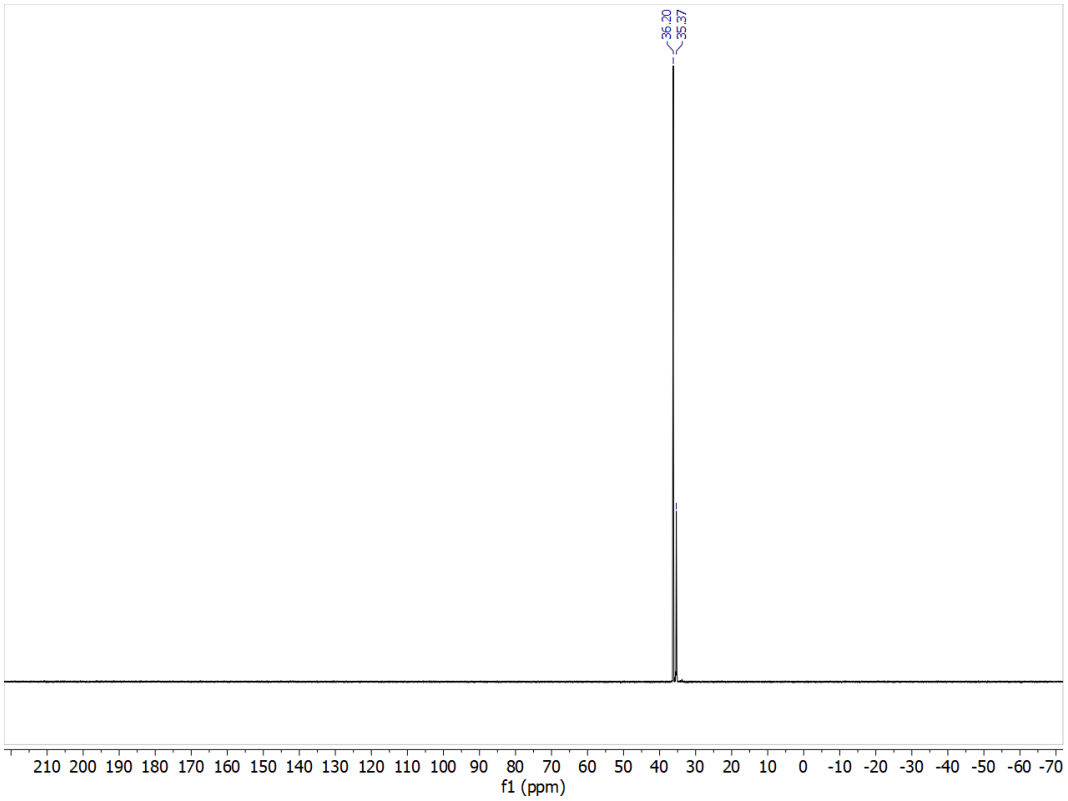

Figure S27. ^{31}P{^{1}H} NMR spectrum (243 MHz, $CDCl_3$) of the equilibrium mixture (1:1) of [PdCl(CH_3)(**H[L2]a**)], **1a**, and [PdCl(CH_3)(**H[L2]b**)], **1b**.

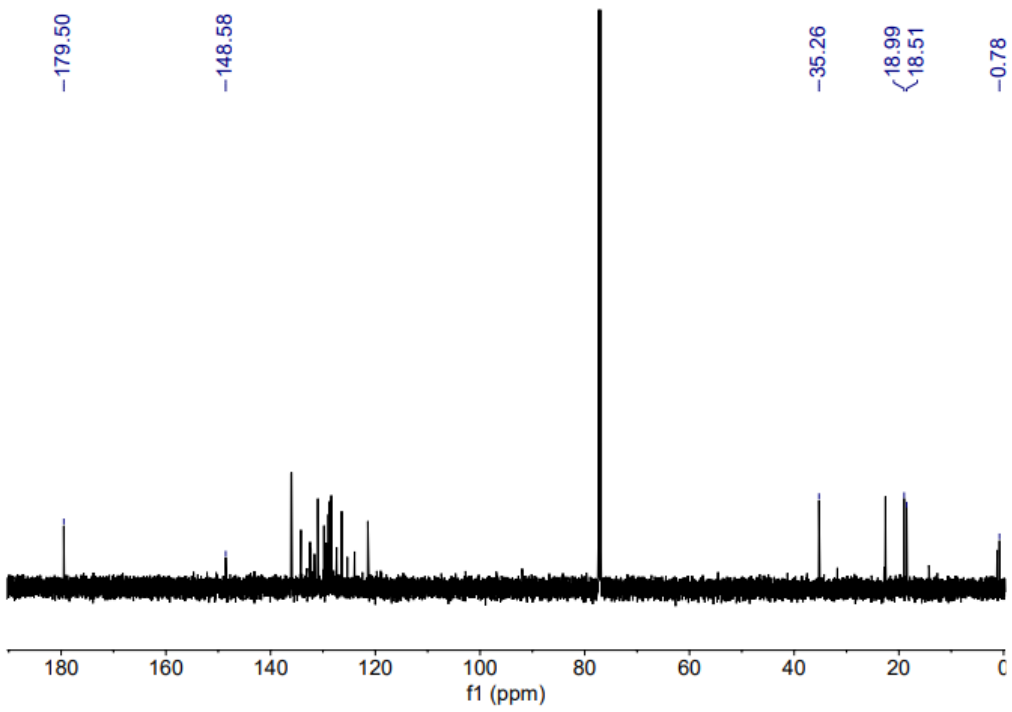

Figure S28. $^{13}C\{^{1}H\}$ NMR spectrum (151 MHz, $CDCl_3$) of the equilibrium mixture (1:1) of [PdCl(CH_3)(**H[L2]a**)], **1a**, and [PdCl(CH_3)(**H[L2]b**)], **1b**. Selected picked peaks correspond to tautomer **1a**.

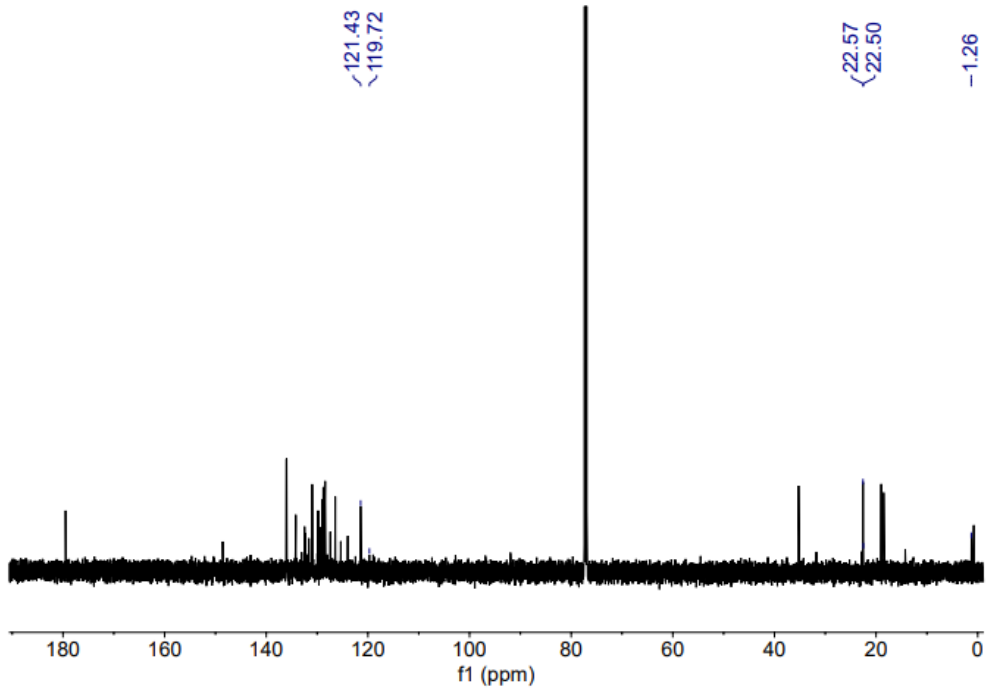

Figure S29. $^{13}C\{^{1}H\}$ NMR spectrum (151 MHz, $CDCl_3$) of the equilibrium mixture (1:1) of [PdCl(CH_3)(**H[L2]a**)], **1a**, and [PdCl(CH_3)(**H[L2]b**)], **1b**. Selected picked peaks correspond to tautomer **1b**.

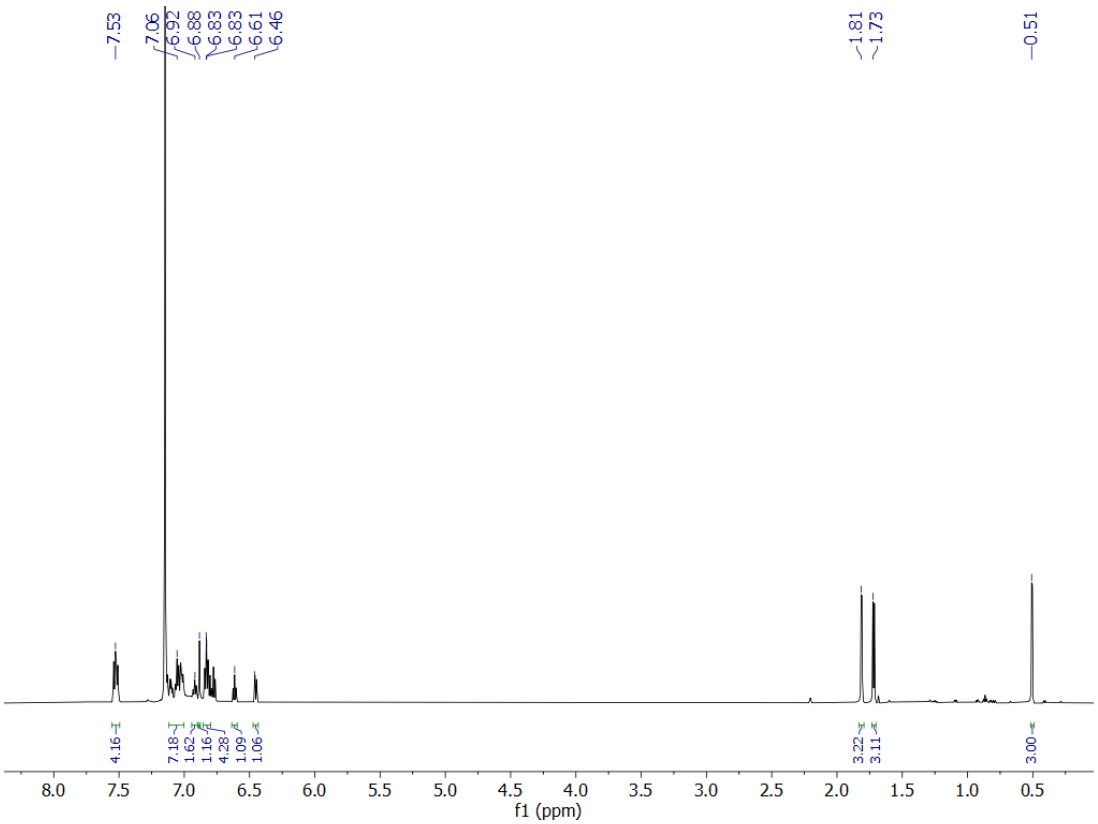

Figure S30. ^{1}H NMR spectrum (600 MHz, C_6D_6) of [Pd(CH_3)(**L2**)], **2**.

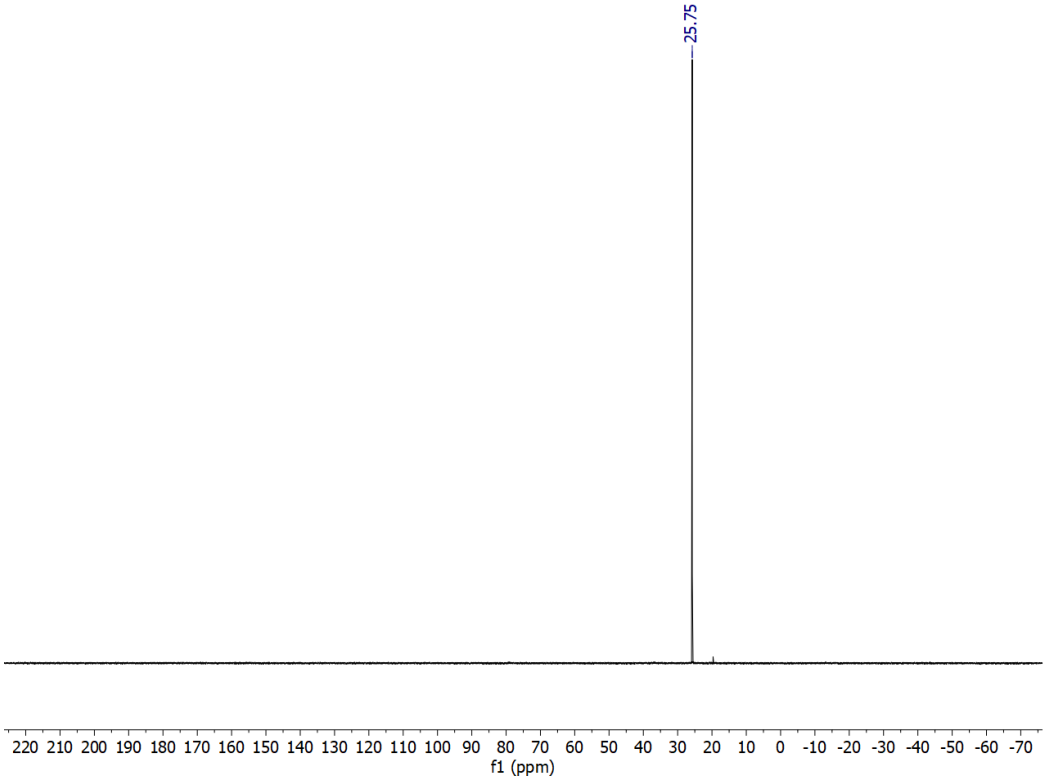

Figure S31. $^{31}P\{^{1}H\}$ NMR spectrum (243 MHz, C_6D_6) of [Pd(CH_3)(**L2**)], **2**.

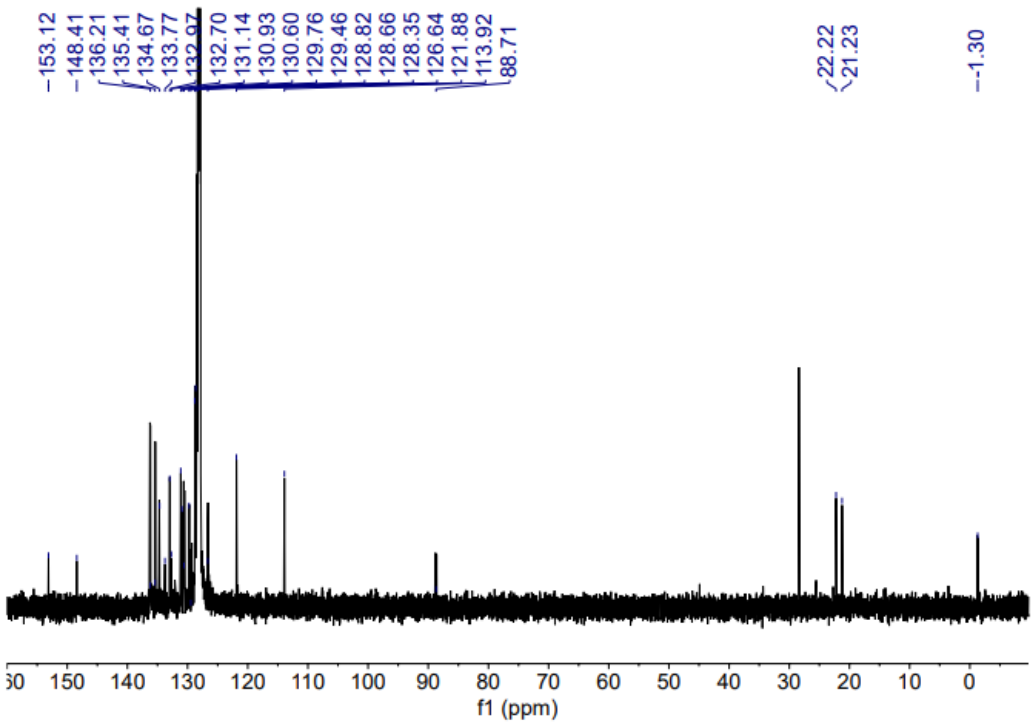

Figure S32. $^{13}C\{^{1}H\}$ NMR spectrum (151 MHz, C_6D_6) of [Pd(CH_3)(**L2**)], **2**.

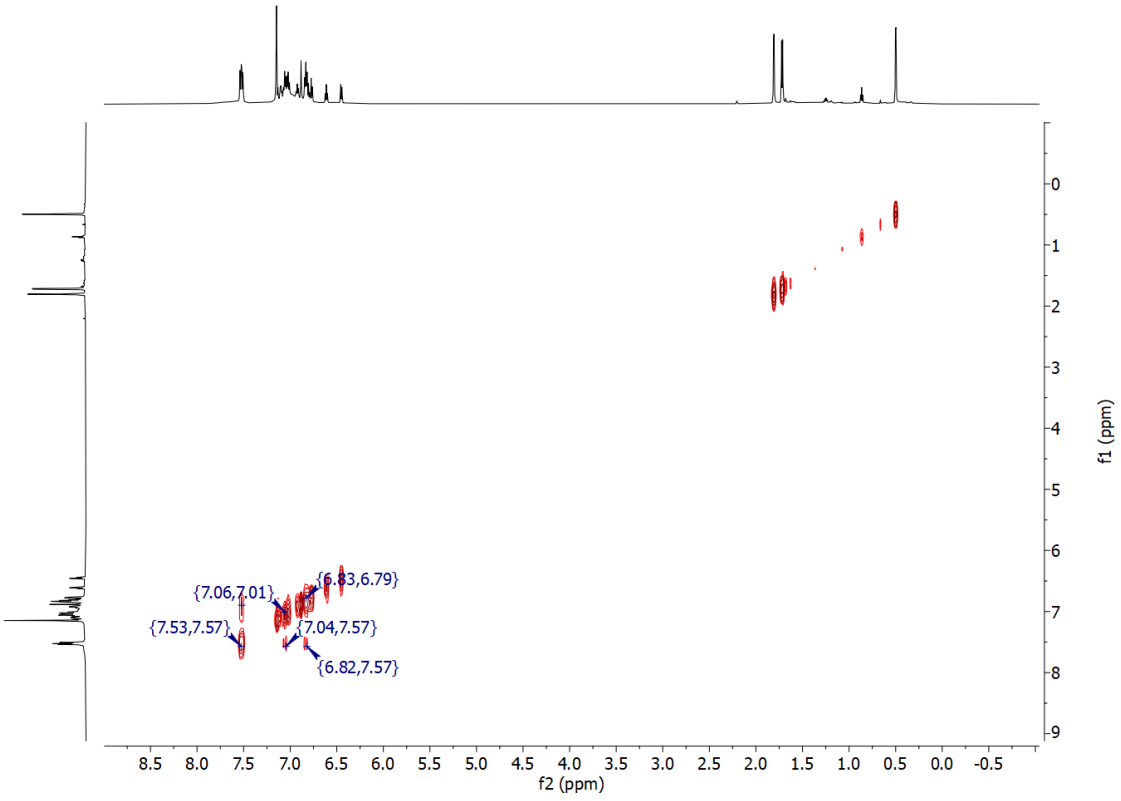

Figure S33. ^{1}H-^{1}H COSY NMR spectrum (600 MHz, C_6D_6) of [Pd(CH_3)(**L2**)], **2**.

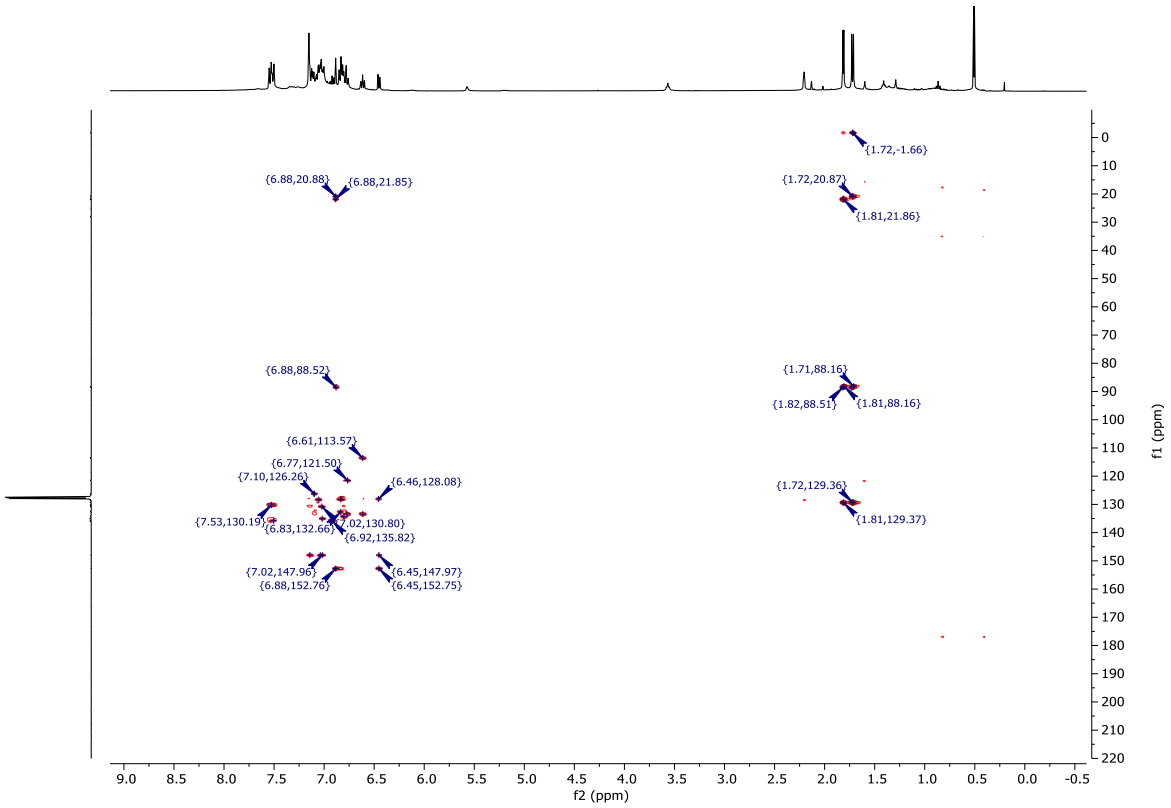

Figure S34. ^{1}H-^{13}C HMBC NMR spectrum (600 MHz, C_6D_6) of [Pd(CH_3)(**L2**)], **2**.

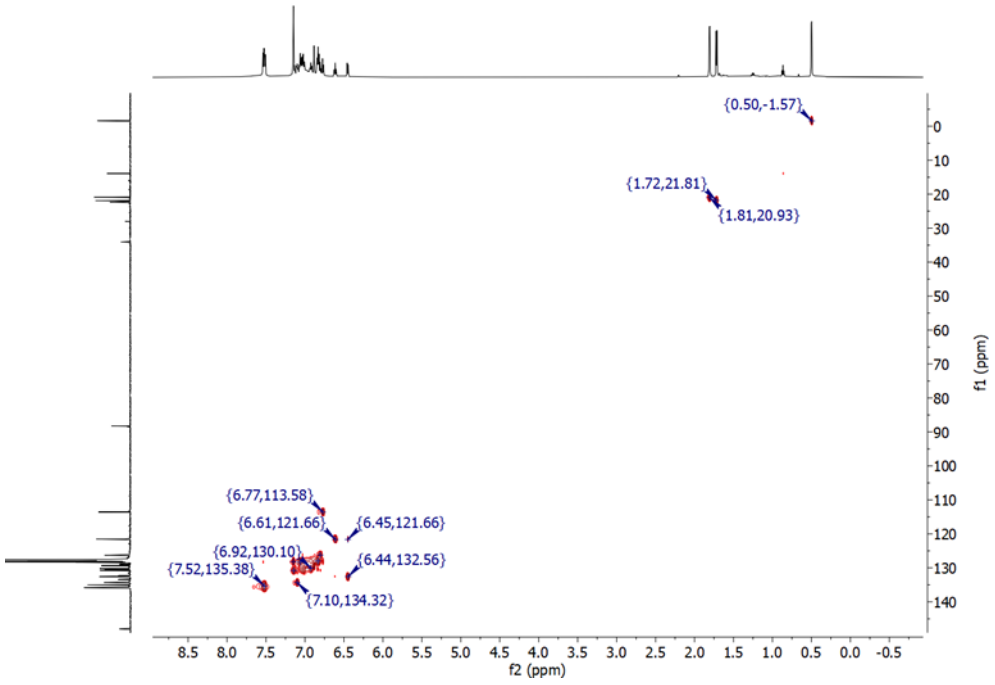

Figure S35. ^{1}H-^{13}C HSQC NMR spectrum (600 MHz, C_6D_6) of [Pd(CH_3)(**L2**)], **2**.

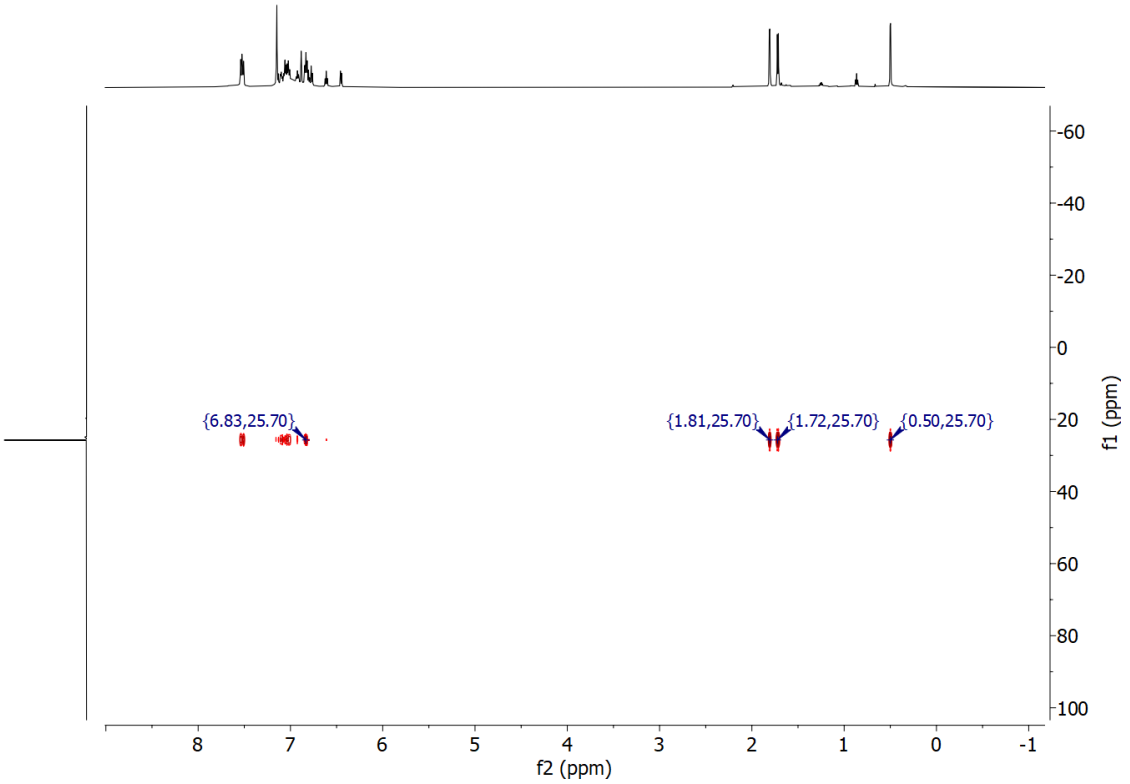

Figure S36. ^{1}H-^{31}P HMBC NMR spectrum (600 MHz, C_6D_6) of [Pd(CH_3)(**L2**)], **2**.

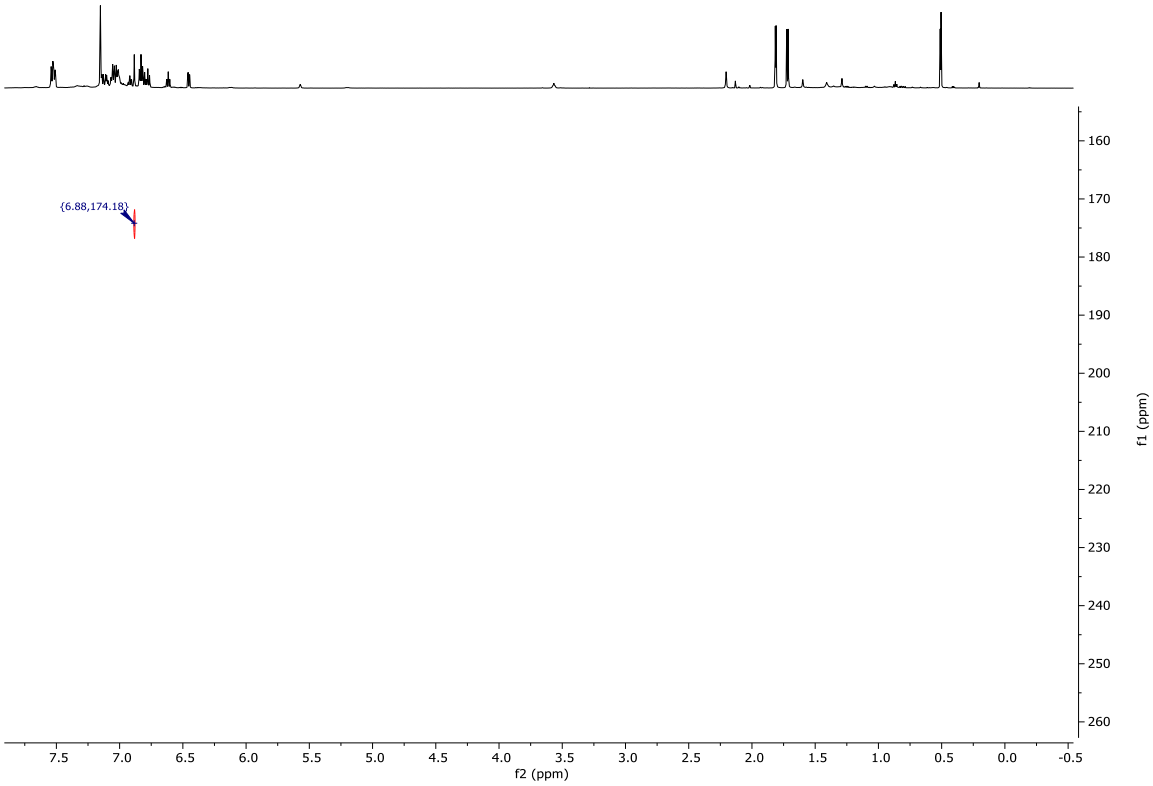

Figure S37. ^{1}H-^{15}N HMBC NMR spectrum (600 MHz, C_6D_6) of [Pd(CH_3)(**L2**)], **2**.

IV – IR Spectra

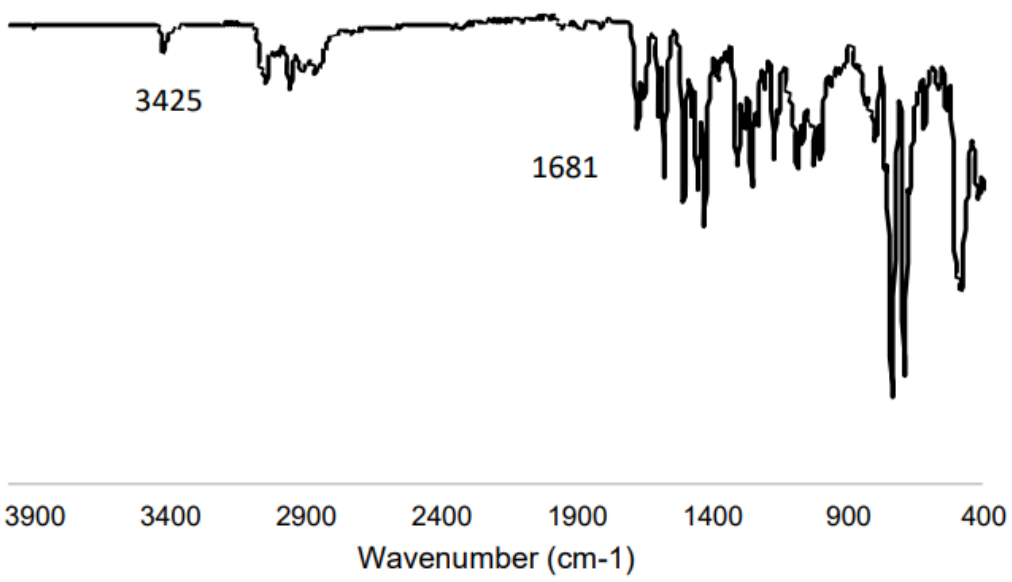

Figure S38. ATR-FTIR of solid $Ph_2P(o\text{-}C_6H_4)(o\text{-}C_6H_4)NCH(i\text{-}Pr)$, **H[L2]a** and $Ph_2P(o\text{-}C_6H_4)(o\text{-}C_6H_4)NHCHC(CH_3)_2$, **H[L2]b**.

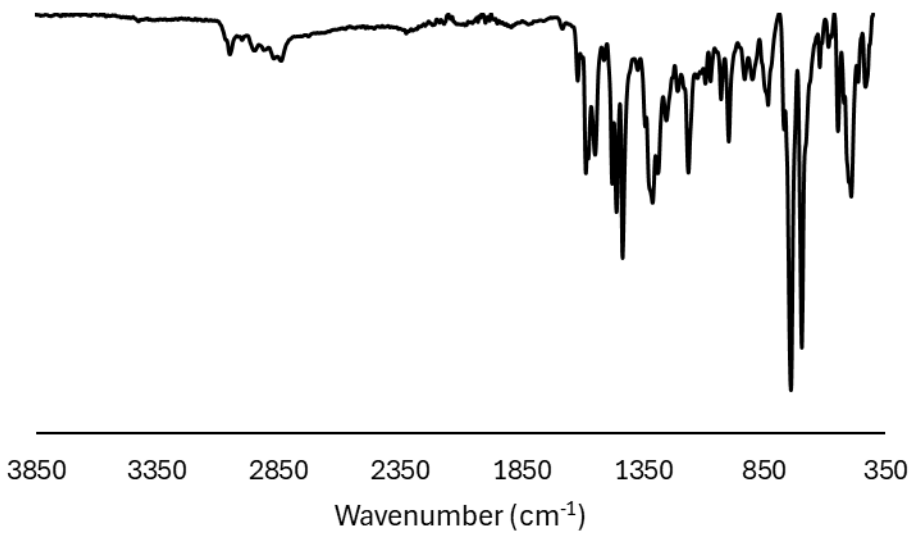

Figure S39. ATR-FTIR of solid $K[Ph_2P(o\text{-}C_6H_4)(o\text{-}C_6H_4)NCHC(CH_3)_2$, **K[L2]**.

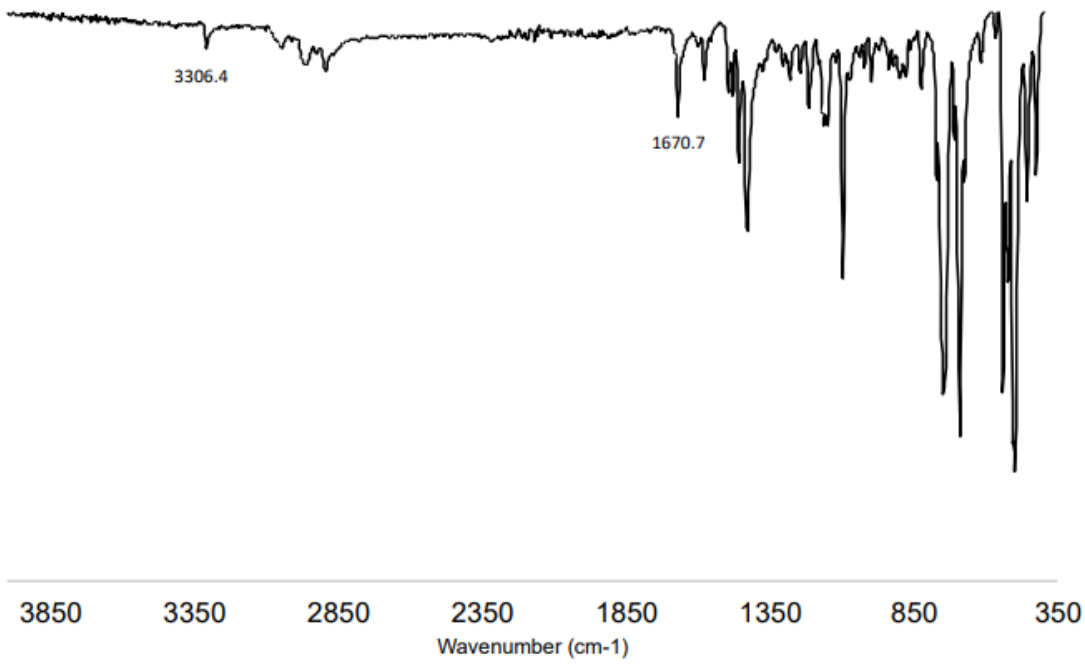

Figure S40. ATR-FTIR of the solid of the tautomeric mixture of [PdCl(CH_3)(**H[L2]a**)], **1a**, and [PdCl(CH_3)(**H[L2]b**)], **1b**.

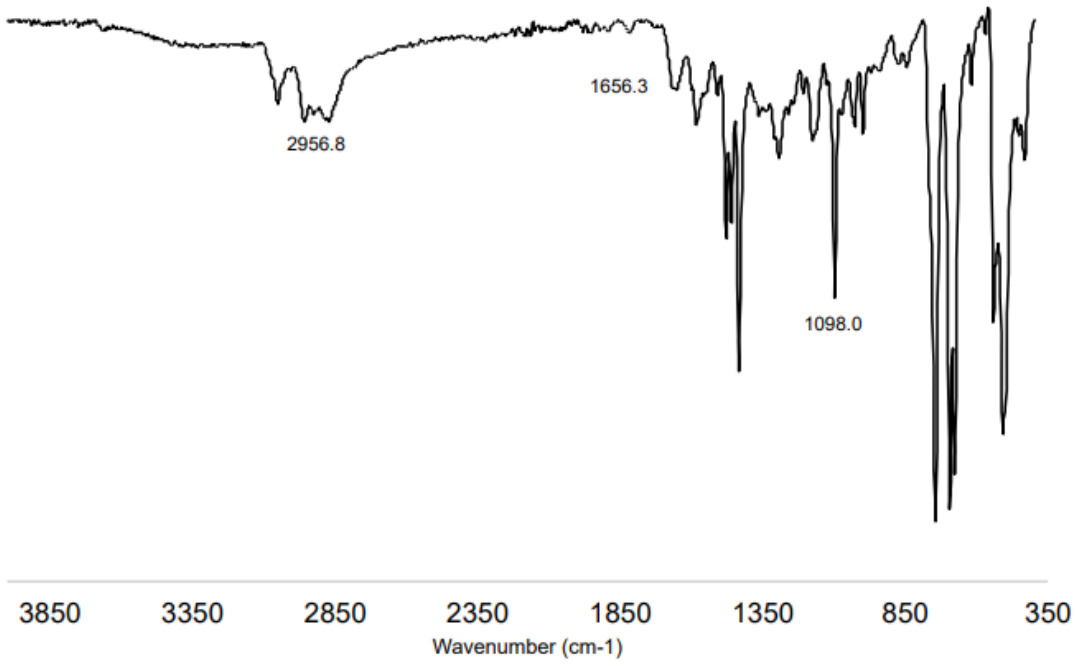

Figure S41. ATR-FTIR of solid [Pd(CH_3)(**[L2]**)], **2**.

V – Mass Spectrometry Data

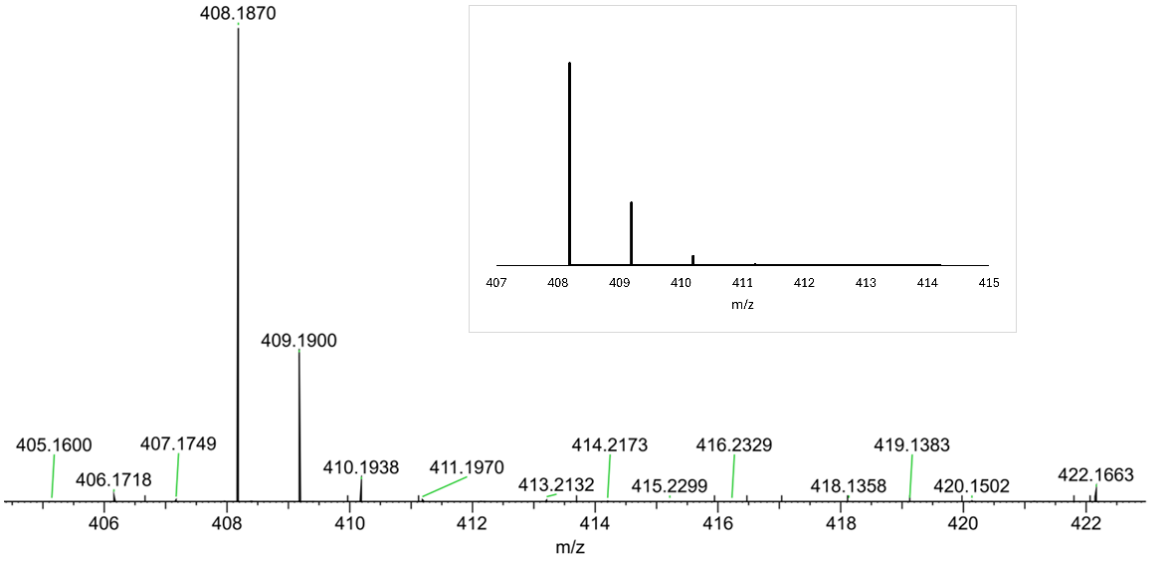

Figure S42. Top: ESI mass spectrum of the tautomeric mixture of $Ph_2P(o\text{-}C_6H_4)(o\text{-}C_6H_4)NCH(i\text{-}Pr)$, **H[L2]a** and $Ph_2P(o\text{-}C_6H_4)(o\text{-}C_6H_4)NHCHC(CH_3)_2$, **H[L2]b**. Observed signal *m/z* = 408.1870. Inset: simulated isotope pattern for $[\mathbf{H[L2]} + H]^+$ ($C_{28}H_{27}NP$) *m/z* = 408.1881.

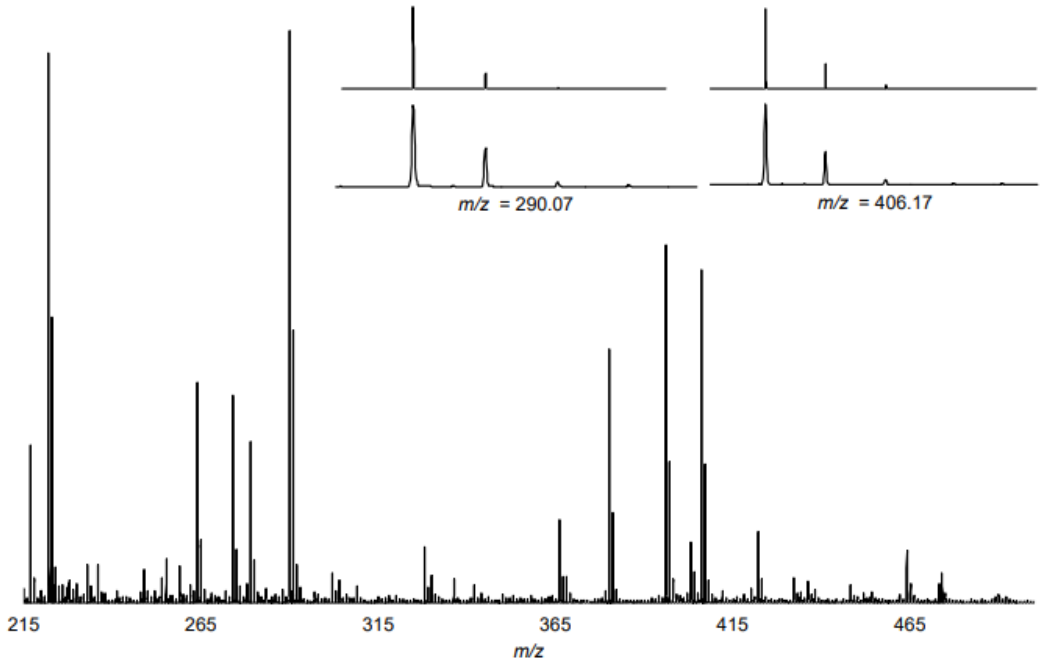

Figure S43. MALDI mass spectrum collected in negative ion mode of $K[Ph_2P(o\text{-}C_6H_4)(o\text{-}C_6H_4)NCHC(CH_3)_2]$, **K[L2]**, with pyrene as the matrix. Left inset: simulated[3] isotope pattern (top) for $[\mathbf{L2} - Ph - (CHC(CH_3)_2)]^-$ ($C_{18}H_{13}NOP$) and observed signal (bottom) at *m/z* = 290.1. Right inset: simulated[3] isotope pattern (top) for $[\mathbf{L2}]^-$ and observed signal (bottom) at *m/z* = 406.2.

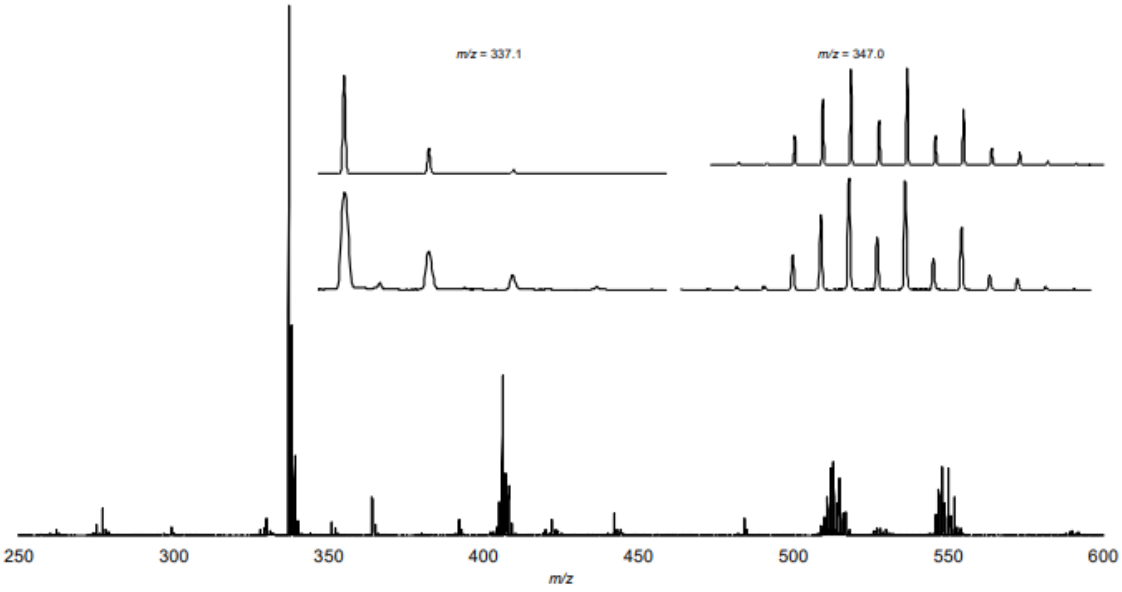

Figure S44. MALDI mass spectrum in positive ion mode of the tautomeric mixture of [PdCl(CH_3)(**H[L2]a**)], **1a**, and [PdCl(CH_3)(**H[L2]b**)], **1b,** with pyrene as the matrix. Left inset: simulated[3] isotope pattern (top) for [**H[L2]** – C_4H_8N]$^+$ ($C_{24}H_{19}P$) and observed signal (bottom) at *m/z* = 337.1. Right inset: simulated[3] isotope pattern (top) for [**1**-CH_3]$^{\bullet+}$ ($C_{28}H_{26}ClNPPd$) and observed signal (bottom) at *m/z* = 548.0.

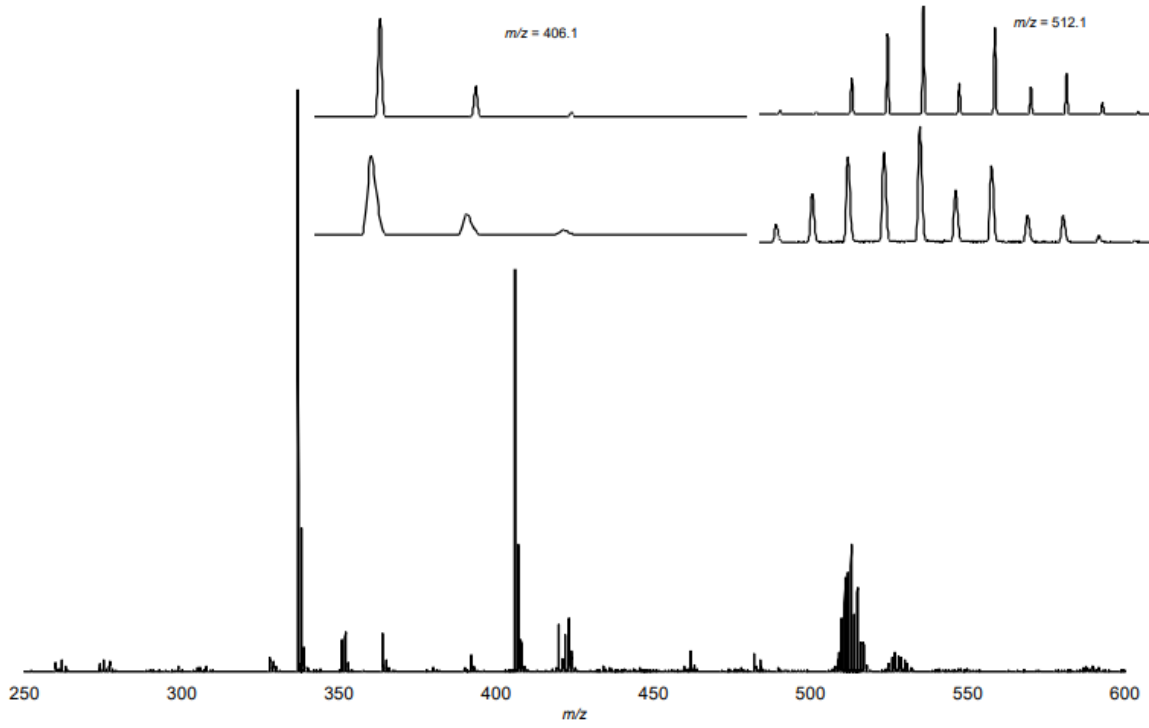

Figure S45. MALDI mass spectrum mode of [Pd(CH_3)(**L2**)], **2** with pyrene as the matrix. Left inset: simulated[3] isotope pattern (top) for [**L2**]$^{\bullet+}$ and observed signal (bottom) at *m/z* = 406.1. Right inset: simulated[3] isotope pattern (top) for [**2**-CH_3]$^{\bullet+}$ ($C_{28}H_{25}NPPd$) and observed signal (bottom) at *m/z* = 512.1.

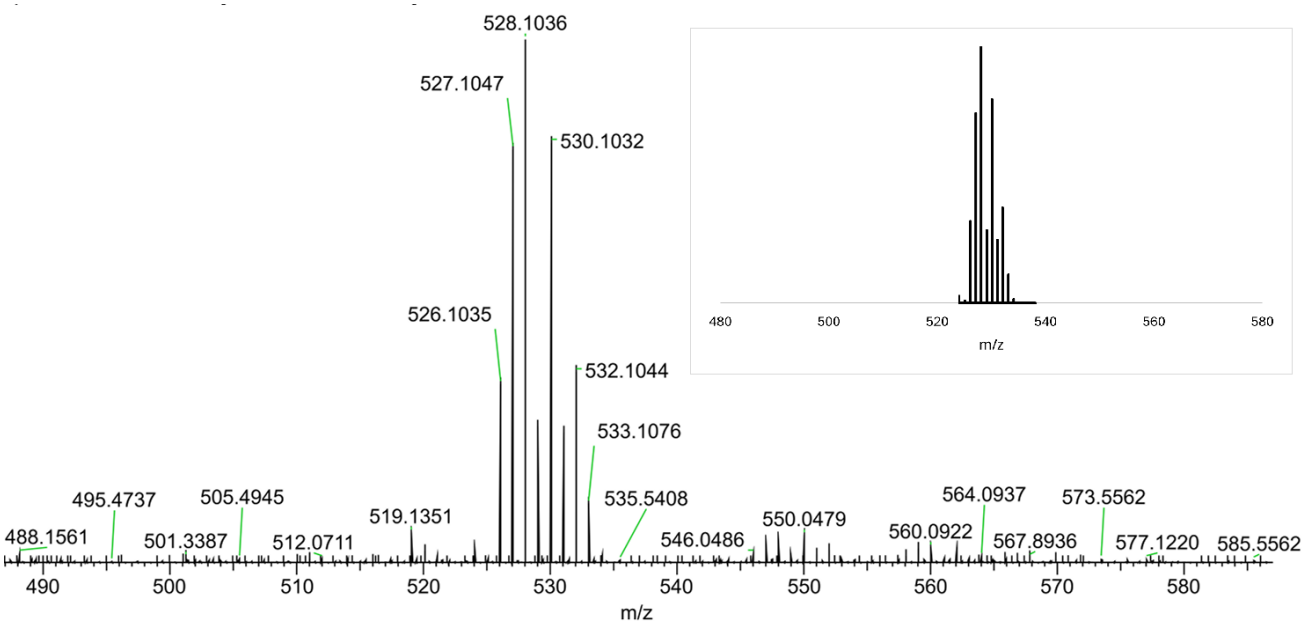

Figure S46. Orbitrap APCI MS in positive ion mode of $[Pd(CH_3)(\mathbf{H[L2]a}) - Cl]^+$ and $[Pd(CH_3)(\mathbf{H[L2]b}) - Cl]^+$, **1a** and **1b**. Inset: Simulated mass spec for the most abundant isotope pattern ($C_{29}H_{29}PdPN$) of $[Pd(CH_3)(\mathbf{H[L2]a}) - Cl]^+$ and $[Pd(CH_3)(\mathbf{H[L2]b}) - Cl]^+$ at *m/z*= 528.1072.

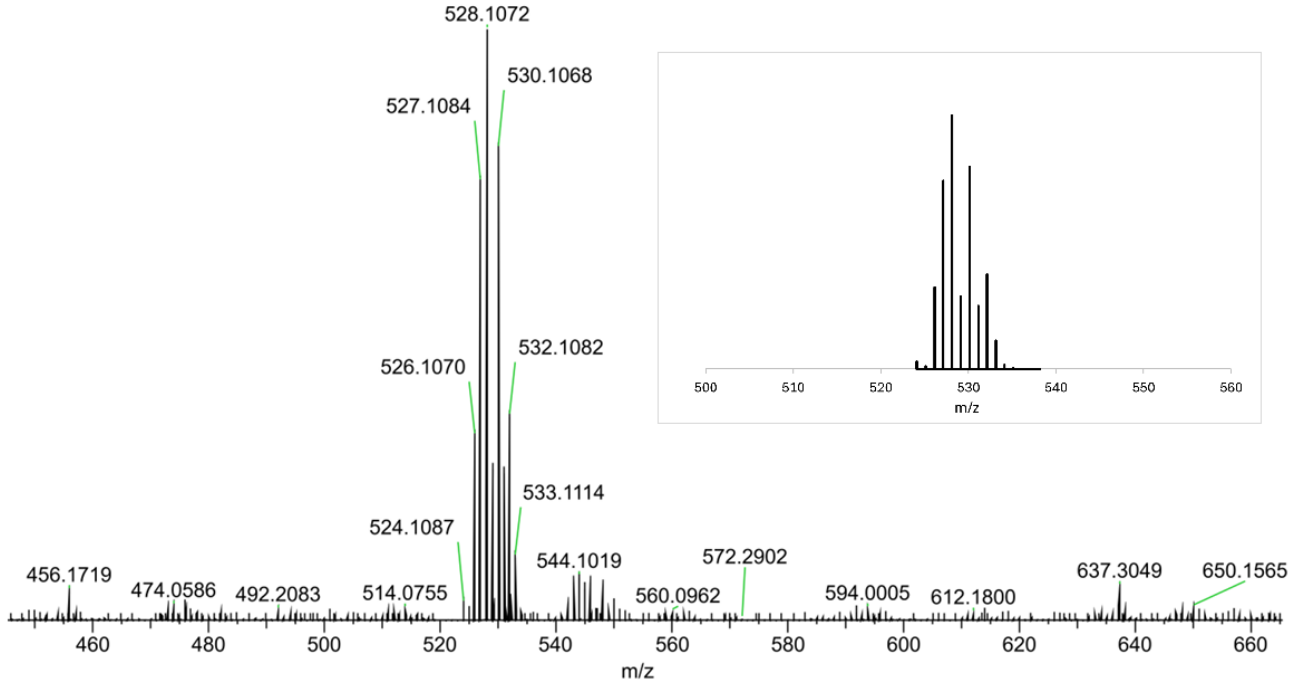

Figure S47. Orbitrap APCI MS in positive ion mode of $[Pd(CH_3)(\mathbf{L2})]$, **2**. Inset: Simulated mass spectra for compound $[\mathbf{2} + \mathbf{H}]^+$ at most abundant observed signal (*m/z* = 528.1072).

VI – UV-Vis Spectroscopy Data

General Procedure for UV-Vis Analysis. All UV-Vis spectra were obtained using the Agilent Technologies Cary 8454 UV-Vis spectrometer at 25 ˚C unless otherwise indicated. A solvent blank was run before each set of samples was run to calibrate the instrument to the selected solvent. All data was plotted using Microsoft Excel.

A stock solution of **2** dissolved in toluene was prepared in a 4 mL vial. Solutions with concentrations of 0.1 mM , 0.2 mM, 0.3 mM, 0.4 mM, and 0.6 mM of **2** were prepared in separate 4 mL vials and the solutions were added to a cuvette equipped with a septum cap. UV-Vis spectra were collected for each concentration.

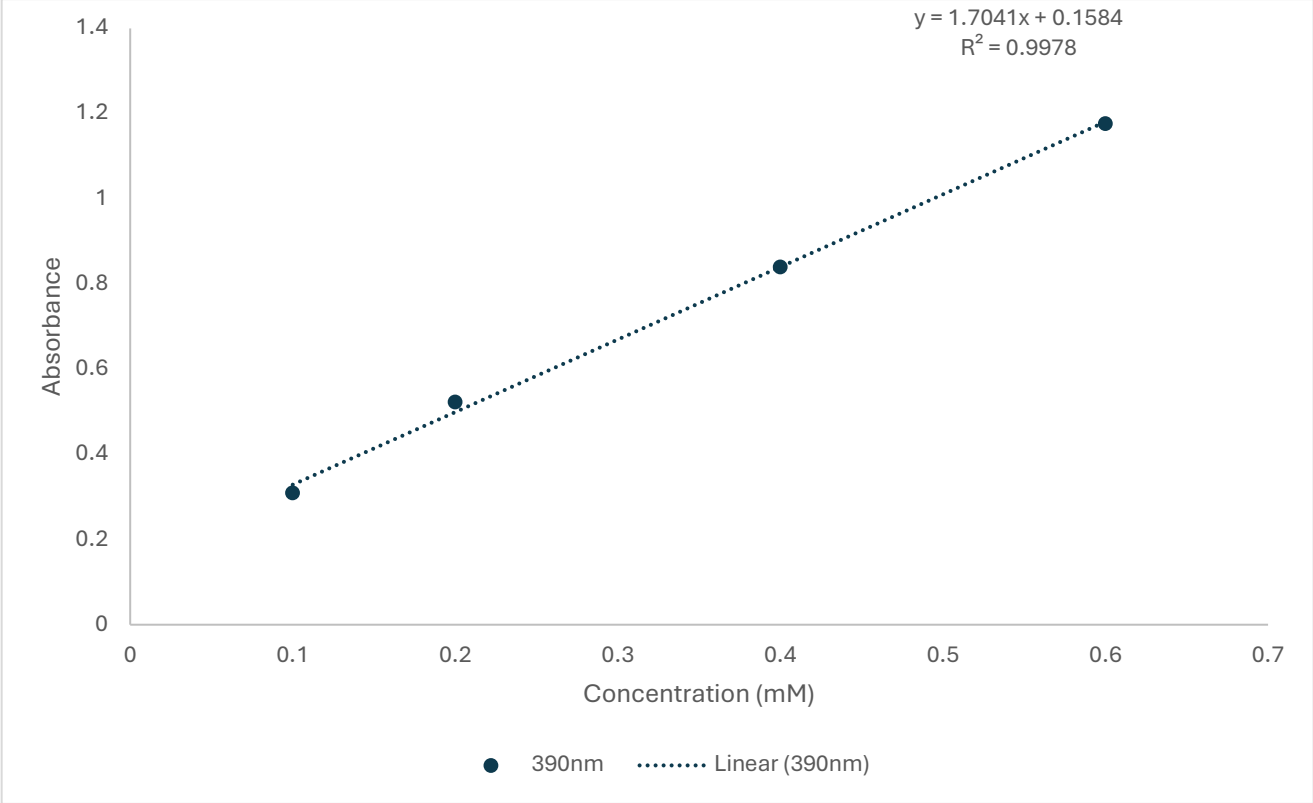

Figure S48. Calibration curve for UV-Vis spectrum of solutions of [Pd(CH_3)(**[L2]**)], **2** in toluene. Absorbance values correspond to that observed at 390 nm for **2** in concentrations of: 0.1, 0.2, 0.4, and 0.6 mM.

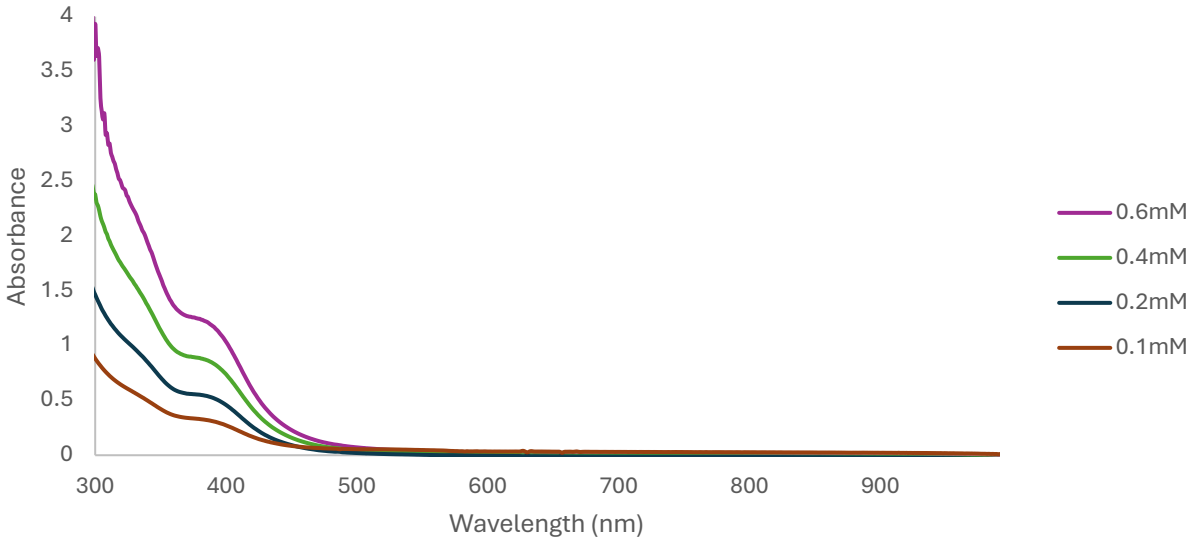

Figure S49. UV-Vis spectra of of solutions of [Pd(CH_3)(**[L2]**)], **2** in toluene.

VII – X-Ray Crystallographic Details

Data Collection and Processing. The sample of **1b** was mounted on a Mitegen polyimide micromount with a small amount of Paratone N oil. All X-ray measurements were made on a Bruker Kappa Axis Apex2 diffractometer at a temperature of 110 K. The unit cell dimensions were determined from a symmetry constrained fit of 9246 reflections with $5.06° < 2\theta < 64.12°$. The data collection strategy was a number of ω and φ scans which collected data up to 72.702° (2θ). The frame integration was performed using SAINT.[4] The resulting raw data was scaled and absorption corrected using a multi-scan averaging of symmetry equivalent data using SADABS.[5]

Structure Solution and Refinement. The structure was solved by using a dual space methodology using the SHELXT program.[6] All non-hydrogen atoms were obtained from the initial solution. The asymmetric unit contained two symmetry independent Pd complexes, designated **A** and **B** and one CH_2Cl_2 molecule of solvation. The hydrogen atoms were introduced at idealized positions and were allowed to ride on the parent atom. The structural model was fit to the data using full matrix least-squares based on F^2. The calculated structure factors included corrections for anomalous dispersion from the usual tabulation. The structure was refined using the SHELXL program from the SHELX suite of crystallographic software.[7] Graphic plots were produced using the Mercury program.[8]

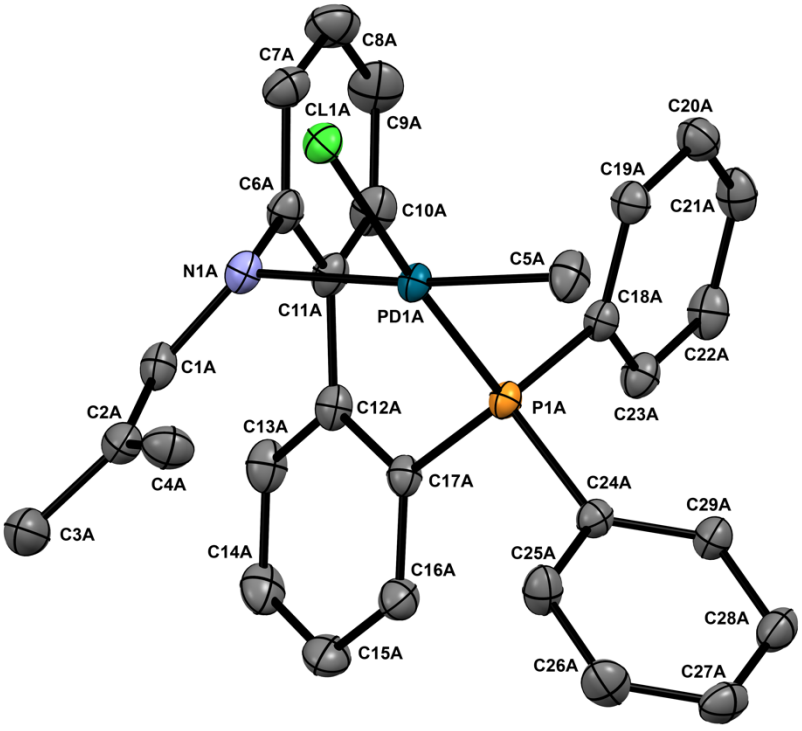

Figure S50. Thermal ellipsoid plot of ***1b molecule A*** showing naming and numbering scheme. Ellipsoids are at the 50% probability level and hydrogen atoms were omitted for clarity.

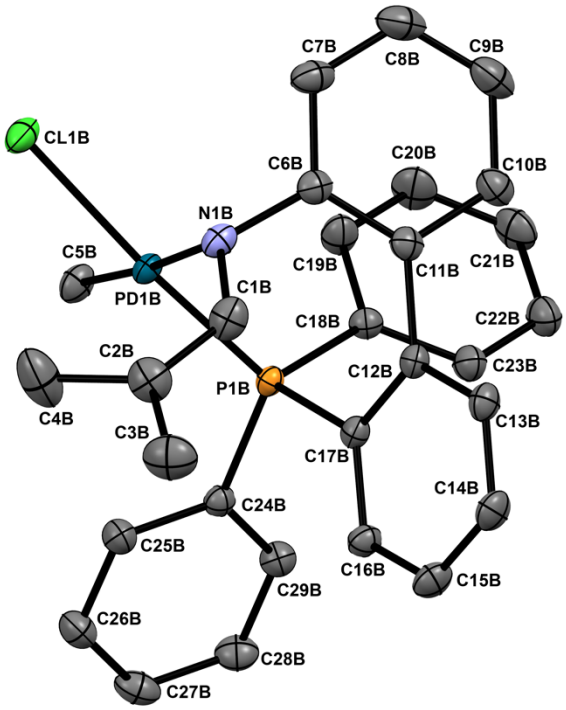

Figure S51. Thermal ellipsoid plot drawing of ***1b molecule B*** showing naming and numbering scheme. Ellipsoids are at the 50% probability level and hydrogen atoms were omitted for clarity.

Table S1. Summary of Crystal Data for **1b**

Formula (CCDC)	$C_{29.50}H_{30}Cl_2NPPd$ (2487843)
Formula Weight (*g/mol*)	606.81
Crystal Dimensions (*mm*)	0.372 × 0.214 × 0.094
Crystal Color and Habit	colourless prism
Crystal System	triclinic
Space Group	P -1
Temperature, K	110
a, Å	10.701(5)
b, Å	14.209(6)
c, Å	18.491(8)
α,°	100.258(10)
β,°	94.936(14)
γ,°	94.487(14)
V, $Å^3$	2744(2)
Number of reflections to determine final unit cell	9246
Min and Max 2θ for cell determination, °	5.06, 64.12
Z	4
F(000)	1236
ρ (*g/cm*)	1.469
λ, Å, (MoKα)	0.71073
μ, (cm^{-1})	0.948
Diffractometer Type	Bruker Kappa Axis Apex2
Scan Type(s)	φ and ω scans
Max 2θ for data collection, °	72.702
Measured fraction of data	0.999
Number of reflections measured	219806
Unique reflections measured	26623
R_{merge}	0.0583
Number of reflections included in refinement	26623

Cut off Threshold Expression	$I > 2\sigma(I)$
Structure refined using	full matrix least-squares using F^2
Weighting Scheme	$w=1/[\sigma^2(Fo^2)+(0.0393P)^2+0.9644P]$ where $P=(Fo^2+2Fc^2)/3$
Number of parameters in least-squares	628
R_1	0.0362
wR_2	0.0813
R_1 (all data)	0.0544
wR_2 (all data)	0.0880
GOF	1.026
Maximum shift/error	0.005
Min & Max peak heights on final ΔF Map (e^-/Å)	-0.905, 0.950

Where:

$R_1 = \Sigma | |F_o| - |F_c| | / \Sigma F_o$

$wR_2 = [\Sigma (w(F_o^2 - F_c^2)^2) / \Sigma (w F_o^4)]^{½}$

$GOF = [\Sigma (w(F_o^2 - F_c^2)^2) / (\text{No. of reflns.} - \text{No. of params.})]^{½}$

VIII – XAS Details

Supplementary Discussion of XAS Data

Pd K-edge EXAFS

Figure S42 is the result of the FT of the EXAFS which is normally denoted χ(k).

χ(k) is the modulation, Δμ, of the absorption coefficient μ when a free atom is placed in a chemical environment, as in a compound, $\Delta\mu = \frac{\mu_{compd} - \mu_{atom}}{\mu_{atom}}$, the absorption coefficient for a free atom is monotonic. When the atom is surrounding by ligands, the photoelectron ejected by an excitation energy > threshold will propagate away from the absorbing atom as a wave with the wavelength described by the de Broglie equation. This outgoing wave will encounter neighboring atoms and will be back scattered (turned around by 180°). This back-scattered wave will interfere with the outgoing wave at the absorbing atom, producing interference which could be in phase of out of phase, resulting in the sinusoidal oscillations in the absorbing coefficient in k space where k is the wave vector and is related to the square root of the kinetic energy of the photoelectron which is E - E_o where E_o is the threshold where the incident photon energy is just enough to excite the core electron into the continuum (vacuum level) and E is the photon energy above the threshold. The chemical information is contained in the backscatter wave's phase and amplitude of the neighboring atom.

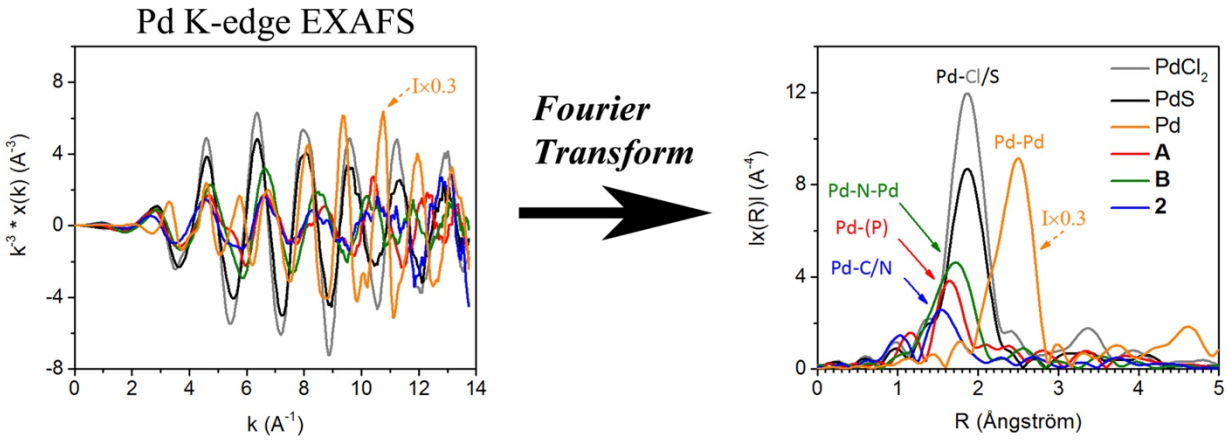

Figure S52. Left panel: Pd K-edge EXAFS of **2**, **A**, **B** and reference compounds Pd metal, PdS and $PdCl_2$ plotted in k space with k^3-weighting. Right panel: the corresponding Fourier Transform in R space. The color legend in the right panel corresponds to the left panel.

The left panel of Figure S42 shows the EXAFS data χ(k) weighted with k^3 (the weighting is to enhanced data at high k, not affecting the FT) before FT. χ(k) = A(k) Φ(k) where A (k) is the amplitude which is based on the nature of the neighboring atom and the interatomic distance, and

Φ(k) is the phase information for the absorbing atom and the backscattering atom. FT can separate these two terms, and the result of FT is a plot of magnitude vs. radial distribution of the neighboring atoms before phase correction (converting data from k space to r space). The phase correction term is typically 0.3-0.4 Å and is a constant for the same absorbing atom and neighboring atom pair (chemical transferability). FT can in principle separate the different waves in R space (Figure S42, right) provided that the backscattering atoms are distinctly different (very different atomic #, Z) and have different bond length.

Note that each absorber-scatterer produces one single sinusoidal oscillation, if the backscattering atoms are with similar Z, the oscillations will have similar pattern leading to a broadening and unresolved (overlapping) interatomic distance in the R space.

Thus, Figure S42 (right) represents the relative bond length of **2**, **A**, and **B**. C/N have very similar phase/amplitude as are P/Cl and they will yield slightly overlapping EXAFS and a slightly broadened peak in the FT. As for the amplitude of the backscattering, in general, the higher the Z, the larger the amplitude as the core electrons are primarily responsible for the back scattering. Compound **B** is a special case where the two bridging N act as a focussing lens, enhancing the amplitude in the FT despite a longer Pd-Pd distance.

P K-edge XANES

The P K-edge XANES probes the LUMO with P 3p/4p character. We can see from Figure S43a that compounds **2**, **A**, and **B** all exhibit a doublet at the edge labelled *a* and *b*. The first derivative display (Figure S43b) reveals a shoulder under peak b; these are well-known resonances in phosphines-metal complexes arising from P 1s to M-P σ*, and to P 1s → P−C σ* and P 1s → P 3p/4p, respectively[9, 10] The similarity among the three spectra indicates that phosphine plays its usual role in the formation of complexes with transition metal ions.

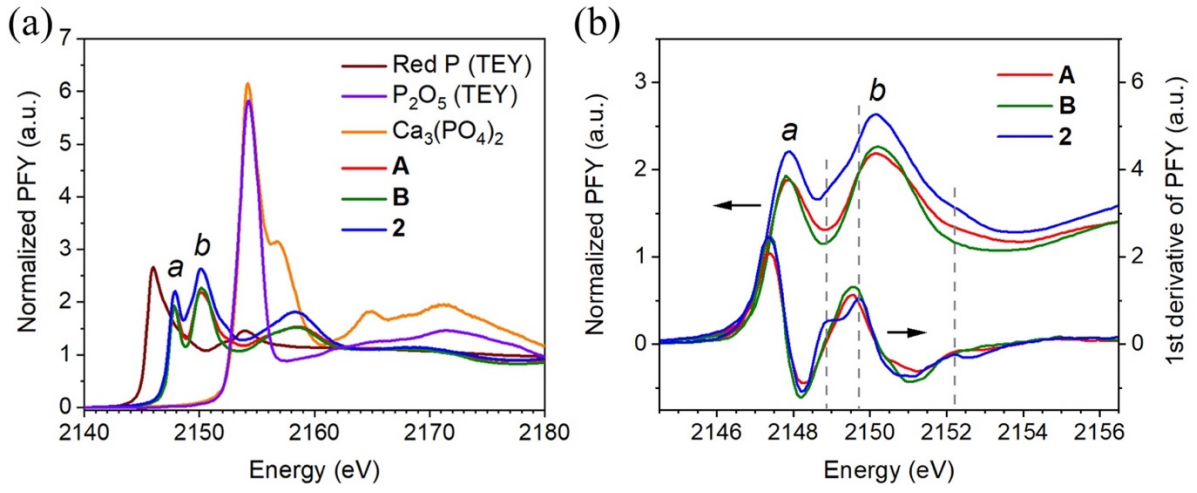

Figure S53. (a) P K-edge XANES of Pd complexes together with P(0) and P(V) standards. (b) The main features at the P K-edge XANES and its first derivative of Pd complexes, showing the local structure from the perspective of the P in phosphine ligands in these complexes.

IX – Summarized Computational Data

All reported thermodynamic state functions are referenced to the ideal-gas standard state of 1 atm for each species, whether solvated or not. This reference pressure corresponds to molar concentrations of $c \approx 0.0409$ M at $T = 298.15$ K and $c \approx 0.0501$ M at $T = 243.15$ K. The experimental concentration of **2** was approximately 0.03 M.

All non-TS structures were verified by vibrational analysis to be true minima.

Table S2. Calculated relative energies (in kJ mol^{-1}) of various structures involving the **L2** ligand. Method: **PBEh-3c** SCRF(PCM,Solvent=Benzene) Int(Grid=SuperFine).

Structure	ΔE_0	ΔG_{243}	ΔG_{298}
2 + **py**	0.0	0.0	0.0
TS	2.9	41.3	49.7
3	–43.6	–2.1	7.2
2-open + **py**	52.1	49.2	48.4
2-dimer[a]	–48.7	–20.3	–13.7

[a] Relative to **2** per mole of monomer

Table S3. Calculated relative energies (in kJ mol^{-1}) of various structures involving the **L2** ligand. Method: **B97-3c** SCRF(PCM,Solvent=Benzene) Int(Grid=SuperFine).

Structure	ΔE_0	ΔG_{243}	ΔG_{298}
2 + **py**	0.0	0.0	0.0
TS	–6.2	31.9	44.9
3	–44.6	–4.1	4.9
2-open + **py**	29.4	26.7	25.8
2-dimer[a]	–64.8	–36.6	–30.2

[a] Relative to **2** per mole of monomer

Table S4. Calculated relative energies (in kJ mol^{-1}) of various structures involving the **L2** ligand. Method: **PBE1PBE/def2-SVP EmpiricalDispersion=GD4** SCRF(SMD,Solvent=Benzene) Int(Grid=SuperFine).

Structure	ΔE_0	ΔG_{243}	ΔG_{298}
2 + **py**	0.0	0.0	0.0
TS	–12.3	24.7	32.8
3	–60.8	–19.6	–10.4
2-open + **py**	43.3	39.7	38.6
2-dimer[a]	–66.1	–38.5	–32.3

[a] Relative to **2** per mole of monomer

Reactant, product, and the transition state:

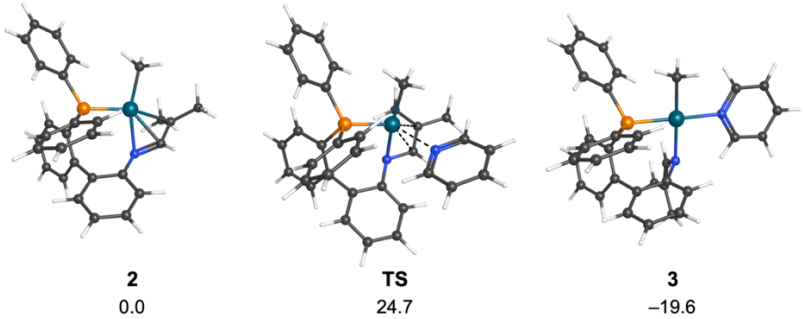

Figure S54. Calculated structures and relative Gibbs energies (ΔG_{243}, kJ mol^{-1}) for **2**, **TS** and **3**, with **2** + **py** as the reference energy. Method: **PBE1PBE/def2-SVP EmpiricalDispersion=GD4** SCRF(SMD,Solvent=Benzene). The corresponding structures optimized using the def2-TZVP basis set (Table 1) are visually indistinguishable.

X – References

1. E. V. Salo and Z. Guan, *Organometallics*, 2003, **22**, 5033-5046.
2. X.-G. Li and Q.-L. Zhou, *Adv. Synth. Catal.*, 2021, **363**, 3471-3475.
3. M. Loos, C. Gerber, F. Corona, J. Hollender and H. Singer, *Anal. Chem.*, 2015, **87**, 5738-5744.
4. Bruker-Nonius, SAINT, version and 2013.8, 2013, Bruker-Nonius, Madison, WI 53711, USA
5. Bruker-Nonius, SADABS, version and 2012.1, 2012, Bruker-Nonius, Madison, WI 53711, USA.
6. G. Sheldrick, *Acta Crystallogr. Sect. A*, 2015, **A71**, 3-8.
7. G. Sheldrick, *Acta Crystallogr. Sect. C*, 2015, **C71**, 3-8.
8. C. F. Macrae, I. J. Bruno, J. A. Chisholm, P. R. Edgington, P. McCabe, E. Pidcock, L. Rodriguez-Monge, R. Taylor, J. van de Streek and P. A. Wood, *J. Appl. Cryst.*, 2008, **41**, 466-470.
9. N. P. Mankad, W. E. Antholine, R. K. Szilagyi and J. C. Peters, *J. Am. Chem. Soc.*, 2009, **131**, 3878-3880.
10. C. M. Donahue, S. P. McCollom, C. M. Forrest, A. V. Blake, B. J. Bellott, J. M. Keith and S. R. Daly, *Inorg. Chem.*, 2015, **54**, 5646-5659.